



**HAL**  
open science

## A chitosan-based nanosystem as pneumococcal vaccine delivery platform

Sandra Robla, Maruthi Prasanna, Rubén Varela-Calviño, Cyrille Grandjean,  
Noemi Csaba

► **To cite this version:**

Sandra Robla, Maruthi Prasanna, Rubén Varela-Calviño, Cyrille Grandjean, Noemi Csaba. A chitosan-based nanosystem as pneumococcal vaccine delivery platform. *Drug Delivery and Translational Research*, 2021, A Perspective of Drug Delivery and Translational Research in Europe, 11 (2), pp.581-597. 10.1007/s13346-021-00928-3 . hal-03313326

**HAL Id: hal-03313326**

**<https://hal.science/hal-03313326>**

Submitted on 3 Aug 2021

**HAL** is a multi-disciplinary open access archive for the deposit and dissemination of scientific research documents, whether they are published or not. The documents may come from teaching and research institutions in France or abroad, or from public or private research centers.

L'archive ouverte pluridisciplinaire **HAL**, est destinée au dépôt et à la diffusion de documents scientifiques de niveau recherche, publiés ou non, émanant des établissements d'enseignement et de recherche français ou étrangers, des laboratoires publics ou privés.

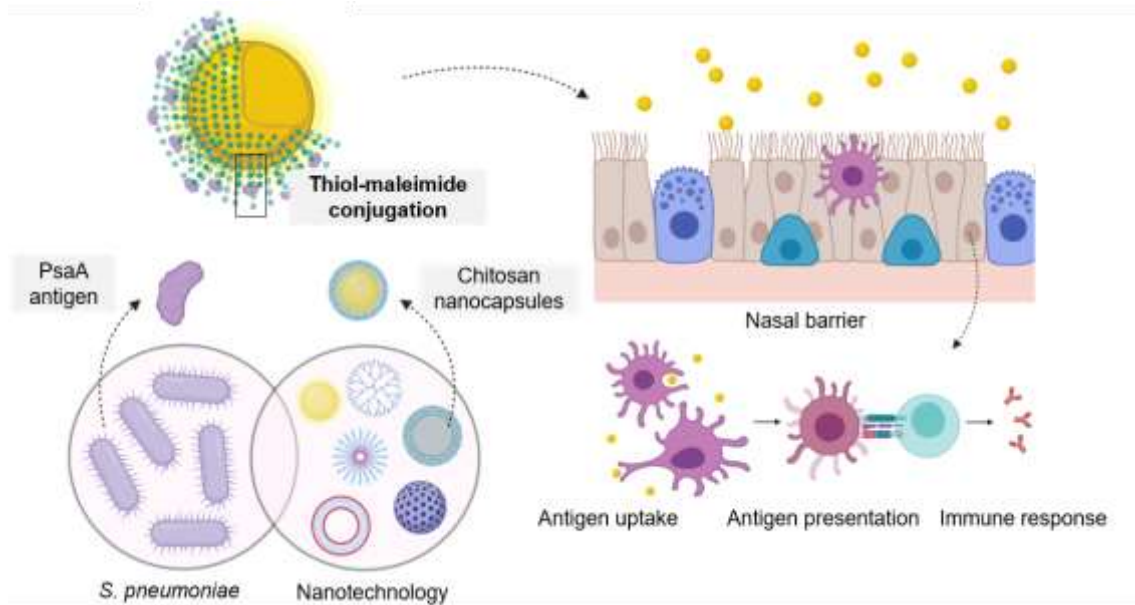
# 1           **A chitosan-based nanosystem as pneumococcal vaccine delivery platform**

2   Sandra Robla, Maruthi Prasanna, Rubén Varela Calviño, Cyrille Grandjean & Noemi Csaba.

## 3   **Abstract**

4   Chitosan-based nanosystems have been described as interesting tools for antigen delivery and for enhancing  
5   the immunogenicity of nasally administered vaccines. As a possible vaccine delivery method, the chemical  
6   conjugation of chitosan nanocapsules with the *Streptococcus pneumoniae* cell membrane protein PsaA  
7   (pneumococcal surface adhesin A) is suggested here. The antigen PsaA, common to all pneumococcus  
8   serotypes, is expected to improve its uptake by immune cells and to activate specific T cells, generating an  
9   adaptive immune response against pneumococcus.

10   With this aim, chitosan nanocapsules with thiol-maleimide conjugation between the polymer (chitosan) and  
11   the antigen (PsaA) were designed to enable the surface presentation of PsaA for immune cell recognition.  
12   Spherical shaped particles, with a size of  $266\pm 32$  nm, positive charge of  $+30\pm 1$  mV and good stability  
13   profiles in simulated nasal fluids (up to 24 h) were achieved. PsaA association rates were three times higher  
14   compared to nanocapsules without covalent polymer-protein conjugation. Cytotoxicity studies in cell  
15   culture media showed non-toxic effect under  $150\ \mu\text{g/mL}$  concentration of nanocapsules, and subsequent  
16   studies on the maturation of immature dendritic cells in the presence of antigen-conjugated nanocapsules  
17   displayed peripheral blood mononuclear cell activation and lymphocyte differentiation after their  
18   presentation by dendritic cells. Secretion of TNF $\alpha$  following exposure to nanocapsules and the ability of  
19   nanocapsules to activate CD4 and CD8 T lymphocytes has also been studied.



20

21 **Graphical abstract:** Antigen loaded nanocarriers uptake and presentation by professional presenting cells.

22 **Keywords:** Chitosan, nanovaccine, dendritic cell, antigen protein, immune response.

23 **1. Introduction**

24 *Streptococcus pneumoniae* is an opportunistic pathogen that colonizes the human upper respiratory tract  
 25 and causes pneumonia, meningitis and septicemia [1]. It is responsible for high morbidity and mortality  
 26 rates, especially among infants, elderly and immunocompromised people [2]. The cell surface of *S.*  
 27 *pneumoniae* contains various proteins and capsular polysaccharides (CPS) that play an important role in  
 28 pathogen attachment and immune system evasion. The CPS diversity results in more than 96 stereotypes  
 29 whereas cell surface proteins are more conserved and less variable [3]. Currently available CPS-based  
 30 vaccines such as PCV13 and PCV10 (Pneumococcal Conjugated Vaccines) and PPSV23 (Pneumococcal  
 31 Polysaccharide Vaccine) only induce specific serotype dependent immune responses [4]. In addition,  
 32 PPSV23 lacks the ability to generate robust immune responses in high-risk populations such as infants or  
 33 the elderly. To address some of these obstacles, several studies investigated the possibility of using protein  
 34 antigens expressed at the *S. pneumoniae* cell wall as potential vaccine candidates. One relevant cell  
 35 membrane protein is Pneumococcal surface adhesin A (PsaA) [5]. PsaA is a critical factor for the  
 36 colonization and adhesion of the pneumococcus in nasopharyngeal epithelial cells. It has been shown to  
 37 activate both the humoral and cellular response of the immune system against the entry of the pathogen via  
 38 the respiratory airways [6].

39 Intranasal route has been extensively explored for non-invasive immunization, stimulating mucosal and  
40 systemic immunity and protecting against respiratory infections [7]. The protective nasal epithelial barrier  
41 presents a large surface area which produces a rapid permeation of drugs [8], as well as the NALT (Nasal  
42 Associated Lymphoid Tissue), responsible for the production of long-term antigen-specific antibodies  
43 [9][10]. The nasal barrier exhibits metabolic activity and is covered with a dynamic mucus layer which  
44 limits the permeability of the epithelium and decreases formulation residence time [11]. In this context,  
45 nanostructures have been described as interesting tools to enhance the delivery of proteins, improving the  
46 immunogenicity of nasally administered vaccines [12]. Indeed, nanostructures play an important role in the  
47 stimulation of an adaptive immune response, upon facilitating the antigen uptake and processing by  
48 professional antigen-presenting cells such as dendritic cells (DCs) [13], and the immediate innate immune  
49 response against these inhaled external substances by macrophages [14]. Chitosan (CS), a polysaccharide  
50 derived from the deacetylation of chitin [15] has been widely used in the design of nanocarriers for nasal  
51 absorption of peptides like insulin, salmon calcitonin, leuprolide or parathyroid hormone [16], thanks to its  
52 high mucoadhesiveness, biocompatibility and biodegradability [17]. Previous studies have shown that  
53 chitosan nanocapsules are good candidates for protein administration by nasal route [16], and also have  
54 been reported to have an adjuvant effect by promoting innate immune responses [18]. In this research, a  
55 mucoadhesive chitosan nanocarrier containing a covalently conjugated pneumococcal protein antigen was  
56 designed and characterized to evaluate its capacity as a nasal drug delivery system..

## 57 **2. Materials and methods**

58 Miglyol 812® was purchased from Cremer Oleo (Hamburg, Germany), polyethylene glycol stearate 40  
59 (PEG-st 40) was purchased from Croda Chemicals Europe Ltd (Snaith, United Kingdom) and sodium  
60 glycocholate (SGC) was obtained from Dextra laboratories Ltd (Reading, United Kingdom). Chitosan HCl  
61 ( $(C_6H_{11}NO_4Cl)_n$ , Mw: 1526.5 g/mol, deacetylation degree of 85%) was purchased from Heppe Medical  
62 Chitosan GmbH (Saale, Germany). 1-Ethyl-3-(3-dimethylaminopropyl) carbodiimide hydrochloride (EDC,  
63  $C_8H_{17}N_3$ , Mw: 191.7 Da), *N*-Hydroxysuccinimide (NHS,  $C_4H_5NO_3$ , Mw: 115.09 Da), sodium chloride  
64 (NaCl), potassium chloride (KCl), calcium chloride hydrate ( $CaCl_2 \cdot 2H_2O$ ) and mucin type III were  
65 purchased from Sigma Aldrich (MO, USA). Maleimide propionic acid 95% (m-PA,  $C_{11}H_{10}N_2O_6$ ,  
66 Mw: 169.13 Da) and hydroxylamine were obtained from Alfa Aesar (MA, USA). Cyanine5 NHS ester dye  
67 (Cy5-NHS) was provided by Lumiprobe (Hannover, Germany), S-acetylthioacetate succinimidyl ester

68 (SATA, Mw: 231.23 Da) and the SnakeSkin™ Dialysis Tubing 3.5K MWCO were obtained from Fischer  
69 scientific (MO, USA). The Ni-NTA resin was obtained from Macherey-Nagel, and PsaA used in the  
70 experiments was provided by UFIP UMR CNRS 6286 at University of Nantes.

71 For *in vitro* experiments sterile and autoclaved material were used. Macrophage Raw 264.7 cell line was  
72 obtained from ATCC (VA, USA), Ficoll-Paque™ PLUS (density 1.077 g/mL) was purchased from GE  
73 Healthcare Bio-Science AB (IL, USA), Roswell Park Memorial Institute medium (RPMI-1640) and  
74 Dulbecco's Modified Eagle's Medium (DMEM) were obtained from GIBCO® (Thermo Fisher Scientific,  
75 MA, USA). Granulocyte-macrophage colony-stimulating factor (GM-CSF), interleukin 4 (IL-4),  
76 allophycocyanin (APC)-conjugated anti-human CD83 (CD83-APC), phycoerythrin (PE)-conjugated anti-  
77 human CD86 (CD86-PE) and fluorescein (FITC)-conjugated anti-human CD1a (CD1a-FITC), were  
78 purchased from Miltenyi Biotec (CA, USA), anti-human CD4-APC, CD8-APC; CD25-PE and CD28-PE  
79 were obtained from Tonbo Biosciences (CA, USA). Fluorescein (FITC)-conjugated anti-human CD3  
80 (CD3-FITC) and phycoerythrin (PE)-conjugated anti-human Tumor Necrosis Factor alpha (TNF- $\alpha$ ) were  
81 both from Miltenyi Biotec (Madrid, Spain). Fetal Bovine Serum (FBS), PSG (100 U/ml penicillin, 0.1  
82 mg/ml streptomycin and 2 mM L-glutamine) and Ebioscience™ 7-aminoactinomycin D (7-AAD) viability  
83 staining were purchased from Invitrogen (CA, USA). Lipopolysaccharide (LPS) from *Escherichia coli* and  
84 Brefeldin A (BFA) were purchased from Sigma Aldrich (MO, USA). MTS (reactive de Owen (3-(4,5-  
85 dinetiltiazol-2-il)-5(3-carboximetoxifenil)-2-(4-sulfofenil)-2H tetrazolium) cell proliferation assay kit was  
86 provided by BioVision (CA, USA). Triton® X-100 was purchased from Scharlab (Barcelona, Spain), and  
87 interferon gamma (IFN $\gamma$ ) was purchased from Peprotech, (London, UK). All other chemicals were of  
88 reagent grade or higher purity.

## 89 2.1. Antigen production and characterization

90 The mature PsaA used as an antigen was previously expressed and purified [19]. Briefly, a plasmid  
91 encoding PsaA deprived of its signal peptide was transformed into *E. coli* BL 21 cells. Fractions containing  
92 the target protein were purified by affinity chromatography and the protein was purified to eliminate any  
93 traces of endotoxin present using endotoxin removal beads.

## 94 2.2. Functionalization of the polymer and proteins and their characterization

### 95 2.2.1. PsaA-SATA conjugation

96 For functionalization of PsaA, 1.35 mg of SATA was incorporated at 45 minute-intervals for 3 times (0.45  
97 mg x 3, ~40 equiv) into 5 mg/mL of PsaA antigen in PBS 0.1 M pH 7.4, at 4°C under stirring. Subsequently,  
98 the reaction mixture was dialyzed in 0.1 M PBS to eliminate the excess of reagent using dialysis membrane  
99 (3.5 kDa) at 4°C. The ability of the conjugated protein to retain its structural conformation was studied  
100 using circular dichroism (CD) using Jasco J-810 spectropolarimeter. The baseline was obtained using a  
101 blank solution containing the buffer. Solution of PsaA or the conjugated PsaA-SATA was diluted to 0.1  
102 mg/mL in buffer solution and was scanned over the wavelength range 200–260 nm. The analysis was  
103 performed using a 1-nm quartz cylindrical cell at a scanning speed of 50 nm/min, 0.1 nm bandwidth and a  
104 temperature of 20°C. PsaA and PsaA-SATA mass spectra were also determined on an Autoflex III MALDI-  
105 TOF/TOF spectrometer (Bruker Daltonics).

#### 106 2.2.2. Chitosan-maleimide conjugation

107 In brief, maleimide-propionic acid (0.553 mg, 5:1 ratio CS:m-PA) in dimethyl sulfoxide (DMSO) was  
108 reacted with 5 mg of chitosan in the presence of 0.339 mg of NHS (2:1 ratio CS:NHS) and 0.188 mg of  
109 EDC (2:1 ratio CS:EDC) as crosslinkers and were kept under constant stirring for 24 h. Excess reagents  
110 were removed by dialysis using dialysis membrane (3.5 kDa). The chemical conjunction between chitosan  
111 and maleimide-propionic acid was confirmed by  $^1\text{H-NMR}$  spectrometry (Bruker BRX-500).

#### 112 2.3. **Preparation of the nanocapsules**

113 Blank CS and CS-maleimide nanocapsules (NCs) were prepared by solvent displacement technique [20].  
114 An organic phase of 1.6 mg of PEG st-40, 0.5 mg of SGC and 6.25  $\mu\text{L}$  of Miglyol<sup>®</sup> (density 0.94 g/mol) in  
115 a final volume of 500  $\mu\text{L}$  of ethanol was poured over a 0.5 mg/mL CS (for CS NCs obtention) or CS-  
116 maleimide (for CS-maleimide NCs) solution [21], and was kept under continuous stirring for 1 h. Later, the  
117 organic solvent was removed under vacuum using rotary evaporation (R-300 Buchi<sup>®</sup>, 150 rpm, 50 mbar, 5  
118 min at 37°C) to a constant volume of 1 mL. Finally, nanocapsules were isolated by centrifugation  
119 (Eppendorf 5430R<sup>®</sup>, at 20.000 g for 30 min at 4°C) and resuspended in ultrapure water.

120 The association of PsaA and PsaA-SATA was carried out at the end of the synthesis of CS and CS-  
121 maleimide nanocapsules, respectively, using a mass ratio of 1:5 (PsaA:polysaccharide) for the association  
122 of the protein. In both cases, protein was added and kept under continuous stirring for 10 min, and to ensure  
123 the entire removal of unassociated PsaA/PsaA-SATA, nanocapsules were centrifugated (10.000 g for 5 min  
124 at RT).

125 For *in vitro* studies, the conjugated NCs were labeled with the fluorescent marker Cy5. For this, Cy5-NHS  
126 in DMSO was added to CS-maleimide in acetate buffer at pH 5.6 (mass ratio 1:1) and kept overnight under  
127 magnetic stirring. Then, the reaction was stopped, and excess dye was removed using PD10 columns  
128 (Centri-Pure P10- Gel Fixing Column, Zetadex-emp Biotech GmbH, Berlin, Germany) and the purified  
129 product was dialyzed again overnight.

130 Optionally, NCs were freeze dried in the presence of trehalose 5% (w/v) as cryoprotectant. NCs and  
131 trehalose solution were mixed 1:1 (v/v) in a freeze-drying glass vials, they were frozen at -80°C and then  
132 transferred to the freeze-drier (Labconco Corp., USA), using a primary drying cycle from -40°C to 20°C  
133 (+10°C/step, 18h, 12h, 5h and 4x2h) and a secondary drying cycle (22°C, 3 h and -20 mTorr vacuum  
134 conditions).

### 135 2.3.1. Physicochemical characterization of nanocapsules

136 The hydrodynamic diameter, polydispersity index (PDI) and derived count rate of the prepared NCs were  
137 measured using dynamic light scattering (DLS). The zeta potential values were obtained by laser droplet  
138 anemometry using a Zetasizer Nano-S (Malvern Instruments; Malvern, UK). The NCs were diluted 1:20 in  
139 ultrapure water (MilliQ®, Merck, NJ, USA) prior to the measurement. Analysis was performed in triplicate  
140 at 25°C with a detection angle of 173° in ultrapure water. Nanoparticle tracking analysis (NTA) was used  
141 to measure the particle size of NCs based on imaging after dilution in ultrapure water using a NanoSight  
142 NS3000 equipment (Malvern analytical Ltd., Malvern, UK). For NTA analysis CS NCs were diluted 1:100  
143 to keep the concentration within the instrument measuring range.

### 144 2.3.2. Association efficiency

145 The association efficiency (AE%) of protein was estimated by quantifying the difference in absorbance of  
146 the total amount of protein and the amount of free protein present in the supernatant after centrifugation.  
147 The free protein in the supernatant was analyzed by Micro BCA assay colorimetric method (Micro BCA  
148 Protein Assay, Thermofisher Scientific, Spain) using a microplate reader (Synergy H1 Hybrid Multi-Mode,  
149 BioTek, Winooski, VT) by measuring the absorbance at 562 nm.

### 150 2.3.3. Morphological characterization

151 The surface morphology of the nanocapsules was studied using FESEM and STEM electron microscopy  
152 (FESEM Ultra Plus, ZEISS, Germany). For FESEM studies, 10 µL of the diluted sample was placed on the  
153 silicon wafer and kept in the desiccator overnight for drying. Before the analysis, the samples were sputter

154 coated with iridium in an argon atmosphere. For STEM studies, NCs were also diluted 1:100 and 10  $\mu$ L  
155 was placed on copper grids with carbon films and then washed drop-by-drop with water. Later the grids  
156 were air dried overnight in the desiccator and the analysis was performed.

#### 157 2.3.4. Colloidal stability

158 The colloidal stability of the antigen loaded nanocapsules before and after freeze drying procedure was  
159 studied *in vitro* using Simulated Nasal Fluid (SNF), composed of 7.45 mg/ml of NaCl, 1.29 mg/ml of KCl  
160 and 0.32 mg/ml of  $\text{CaCl}_2 \cdot 2\text{H}_2\text{O}$  and pH adjusted at 6.5. SNF supplemented with mucin type III (1% sialic  
161 acid content) at 0.1% was also used for the study. For further studies in dendritic cell culture, the stability  
162 of the nanosystems was assessed in cell culture RPMI-1640 medium, following the change in particle size,  
163 mean count rate and PDI over a period of 24 h. In brief, 20  $\mu$ L of NCs were mixed with 980  $\mu$ L of SNF with  
164 0.1% mucin or 980  $\mu$ L of RPMI, while nanoparticles suspended in SNF and water at same concentrations  
165 are used as controls. The NCs in the different media were shaken at 100 rpm at 37°C using a constant-  
166 temperature shaker, at different time points (0, 6 and 24 h) the size and count rate of samples were measured  
167 using DLS as described in Section 2.3.1.

#### 168 2.4. **Release studies**

169 *In vitro* release studies of PsaA from the conjugated nanocapsules was performed by incubating non-  
170 conjugated CS-PsaA and conjugated CS-maleimide PsaA nanocapsules in a final volume of 1 mL of SNF  
171 in a shaking incubator (Biosan Thermo-Shaker TS-100C, 600 rpm at 37°C). At different time intervals (1,  
172 3, 5, 8, 12 and 24 h), samples were centrifuged (5 min at 10,000 g and RT) and 250  $\mu$ L of supernatant were  
173 collected for analysis and replaced with fresh SNF medium to maintain sink conditions [22]. The amount  
174 PsaA contained in the supernatant at scheduled time intervals were subsequently analyzed by absorbance  
175 measurement in a multilabel plate reader using BCA assay at 562 nm.

#### 176 2.5. **Blood samples and dendritic cell preparation**

177 Heparinized blood samples were obtained from healthy donors after informed consent. The *buffy coats*  
178 from anonymous donors were donated by the Organ and Blood Donation Agency (ADOS; Santiago de  
179 Compostela, Spain). The peripheral blood mononuclear cells (PBMCs) were isolated using Ficoll gradient  
180 centrifugation method [23]. Briefly, blood was diluted with PBS (1:1) and layered onto Ficoll-Paque™  
181 PLUS at a ratio of 2:1 (blood:Ficoll). Different components were isolated after centrifugation (Allegra X-  
182 12R, Beckman Coulter) at 400 g for 30 min at RT, and PBMCs were collected from the interface, washed

183 twice with PBS and centrifuged again (300 g, 10 min at RT). Cells were resuspended in R<sub>2</sub> medium (RPMI-  
184 1640 supplemented with 2% heat-inactivated FBS and 1% of PSG). The density was adjusted to 1×10<sup>6</sup>  
185 cells/mL and 10 mL of cells were seeded into 75 cm<sup>2</sup> cell culture flask for 2 h (37°C, 5% CO<sub>2</sub>). After the  
186 incubation period, non-adherent cells (peripheral blood lymphocytes or PBLs) were washed with PBS and  
187 attached monocytes were cultured for another 6 days, renewing half of the medium after three days, in R10  
188 medium (RPMI-1640 supplemented with 1% antibiotics and 10% FBS) in the presence of IL-4 and GM-  
189 CSF (both at 100 ng/mL) to allow the cells to differentiate into DCs [24][25].

## 190 2.6. NCs toxicity on immune cells

### 191 2.6.1. MTS assay

192 The cytocompatibility of the antigen loaded CS-maleimide PsaA NCs with the dendritic cells was studied  
193 using MTS assay, and the presence of the soluble formazan product was determined by measuring the  
194 absorbance that is directly proportional to the number of viable cells [26]. Monocyte differentiated  
195 immature DCs (iDCs) were added into 48-well microplate (1×10<sup>6</sup> cells/mL) and blank CS-maleimide and  
196 CS-maleimide PsaA NCs with a concentration range from 400 µg/ml to 25 µg/ml were incorporated. As a  
197 negative control (0% toxicity), iDCs in culture medium was used, whereas, for the positive control (100%  
198 toxicity), iDCs were incubated with Triton X-100 (0.5%). In the same manner, macrophage Raw 264.7  
199 cells were incubated with blank CS-maleimide and CS-maleimide PsaA NCs and treated using the same  
200 procedure as iDCs. After 4 and 24 h of incubation under standard sterile conditions for cell culture (37°C  
201 and 5% CO<sub>2</sub>), cells were collected and centrifuged (Microfuge 5427-R, Eppendorf, 500 g, 5 min at RT) for  
202 the removal of un interacted nanocapsules. Finally, the cells were incubated with 10 µL of MTS reagent  
203 and the absorbance was measured at 490 nm using a microplate reader.

### 204 2.6.2. 7-AAD assay

205 Cytotoxicity studies on the dendritic cells were also carried out using the intercalative DNA fluorescent  
206 dye 7-AAD. iDCs were incubated for 24 h with different CS-maleimide PsaA NCs concentrations from  
207 900 µg/mL to 50 µg/mL and after the incubation period, cells were washed and stained with 0.05 µg/µL of  
208 7-ADD (30 min at 4°C) for analysis by flow cytometry (BD FACSCalibur™, Becton Dickinson). The  
209 emission of 7-AAD was detected in the FL-3 channel at 650 nm. The analysis was performed with Flowing  
210 software (Cell Imaging Core, Turku Biotechnology Center, Turku, Finland) [27].

## 211 2.7. Interaction of NCs with immune cells

212 The analysis of the uptake of CS-maleimide PsaA NCs by the DCs and Raw 264.7 cells was processed by  
213 means of confocal laser scanning microscopy (CLSM) and FESEM microscopy, respectively. For CLSM,  
214 DCs were incubated with Cy5-labeled nanosystems at a concentration of 150  $\mu\text{g}/\text{ml}$  and they were  
215 visualized by confocal microscopy (Leica SP5, Mannheim, Germany) after 24 h. For FESEM analysis, Raw  
216 264.7 cells were seeded on a poly-L-Lysine coated cellware (Corning Life Sciences, MA, USA) and  
217 nanocapsules were added, and allowed to incubate for 24 h. Later, the cells were fixed using 4%  
218 paraformaldehyde (PFA), washed and gradually dehydrated using increasing ethanol concentrations (30%,  
219 70%, 96%, 100%). Cells were placed in the desiccator overnight and were sputter coated with iridium  
220 before visualization [26].

## 221 2.8. Human DCs phenotype analysis

222 iDCs were incubated with the conjugated CS-maleimide PsaA NCs at a final concentration of 150  $\mu\text{g}/\text{ml}$   
223 during 48 h. Cells were washed twice (400g, 6 min at RT) to eliminate excess NCs, resuspended in PBS  
224 and stained with optimal amounts of different antibodies (CD11a-FITC, CD83-APC and CD86-PE) for 25  
225 min at RT, in the dark. Finally, levels of maturation markers were quantified by flow cytometry.

## 226 2.9. NCs tolerogenic effect in immature DCs

227 2,3-Indoleamine dioxygenase (IDO) expression was evaluated in iDCs maturation after conjugated CS-  
228 maleimide PsaA NCs exposition. In brief, 1.25  $\mu\text{l}$  of L-tryptophan (100  $\mu\text{M}$ ) was added to the iDCs medium  
229 during the last 4 h of incubation. Then, cells were centrifuged (1,000 g, 5 min at RT) and supernatants were  
230 mixed with 30% trifluoroacetic acid (2:1 v/v) and centrifuged again (10,000 g, 5 min, RT). The supernatant  
231 was mixed with the Ehrlich Reagent (1:1 v/v) and absorbance at 490 nm was determined using a microplate  
232 reader as indicated.

## 233 2.10. Activation of CD4 and CD8 T cells by NCs

234 After total monocyte differentiation into iDCs, they were harvested, resuspended in R10 medium and iDCs  
235 ( $1 \times 10^6$  cells/mL) were co-incubated with 150  $\mu\text{g}/\text{ml}$  of blank CS-maleimide NCs, CS-maleimide PsaA NCs  
236 and PsaA. As a negative control (no activation), iDCs in culture medium were used, whereas for the positive  
237 control (total activation), mature DCs (mDCs) were obtained by incubation of iDCs with bacterial LPS (20  
238 ng/ml) and IFN- $\gamma$  (200 IU/ml). After 48 h, cells were harvested and centrifuged to remove nanocapsules  
239 (300 g, 10 min at RT). In parallel, allogenic PBLs were obtained from *buffy coats* after 2 h of PBMCs  
240 incubation with R2 medium and they were co-incubated with DCs for 12 days, renewing culture media and

241 splitting the cells as necessary (usually every 2-3 days). Non-adherent cells were collected and centrifuged  
242 (500 g for 5 min at RT), washed and divided into two different groups. CD4-APCs together with CD25-PE  
243 (5  $\mu$ L/each) were added to the first, while CD8-APCs together with CD28-PE (5  $\mu$ L/each) were added to  
244 the latter and left to incubate at 4°C for 25 min in darkness. After incubation, cells were washed and  
245 centrifuged (400 g for 6 min at RT) for their analysis by flow cytometry as described above.

#### 246 2.11. Cytokine secretion by PBMCs incubated with different NCs

247 PBMCs ( $1 \times 10^6$  cells/mL) were collected from healthy donors and incubated with blank CS-maleimide NCs,  
248 CS-maleimide PsaA NCs and PsaA alone (150  $\mu$ g/mL) (5% CO<sub>2</sub>, 37 °C) for 2 h. After that, cells were  
249 washed and centrifuged (300 g for 10 min at RT), thus removing the nanocapsules. Then, BFA (10 mg/ml,  
250 5  $\mu$ L/well) was added to block the secretion of cytokines and kept for overnight incubation. The following  
251 day, cells were centrifuged again under the same conditions, the PBMCs surface was stained with CD3-  
252 FITC (10  $\mu$ L/well) antibody and left for 15 min at 4°C in darkness. Cells were washed, centrifuged (400 g,  
253 6 min at RT) and fixed with 1% PFA under constant agitation to avoid cell aggregation, and were incubated  
254 again for 15 min in darkness. Cell membrane was permeabilized with 1% saponin and centrifuged again  
255 under the initial conditions for an intercellular staining with TNF $\alpha$ -PE cytokine antibody (5  $\mu$ L/well) and  
256 incubated for 15 min at 4°C in darkness. Finally, cells were washed twice with 0.1% saponin buffer and  
257 fluorescence signals were measured by flow cytometry as indicated.

#### 258 2.12. Statistical analysis

259 Results were expressed as mean  $\pm$  standard deviation (SD) and mean  $\pm$  standard error mean (SEM) for  
260 dendritic cells studies. Data analyses were carried out using GraphPad Prism v.6.01 software (GraphPad  
261 Software Inc., San Diego, CA, USA). Statistical analyses using the 2-way ANOVA test in combination  
262 with Dunnett's multiple comparisons test were used to determine the difference between donor groups.

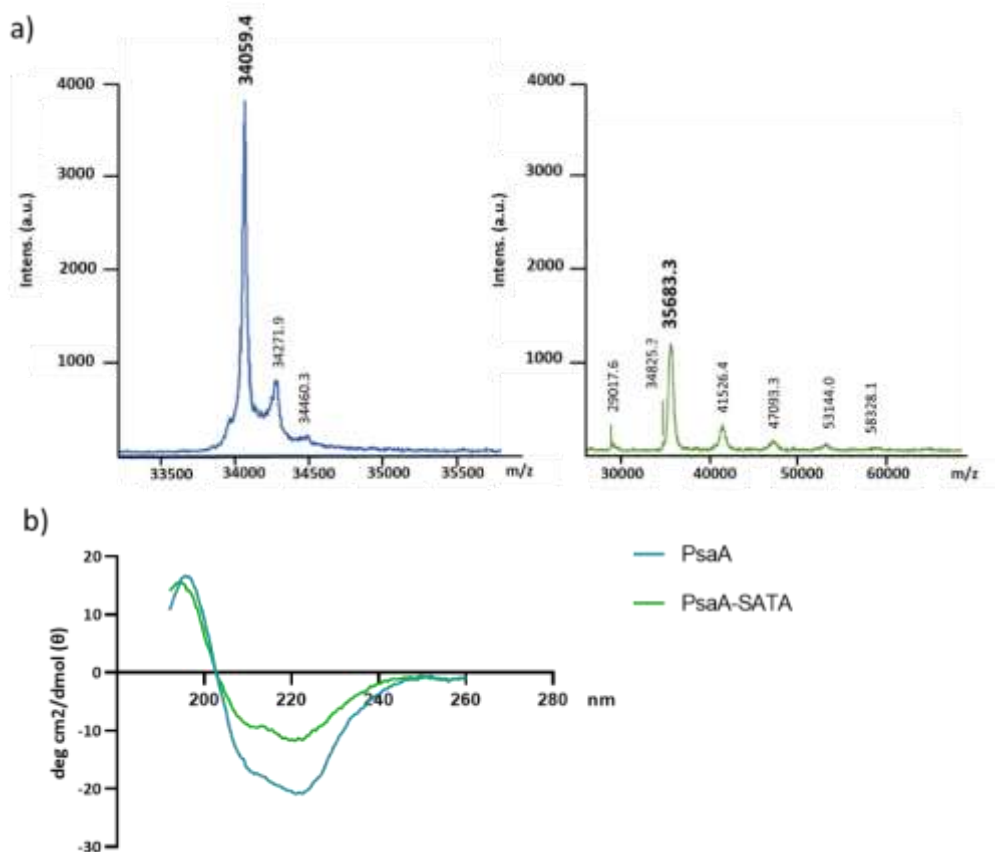
### 263 3. Results and discussion

#### 264 3.1. Functionalization of the polymer and protein and their characterization

##### 265 3.1.1. PsaA-SATA conjugation

266 In the search for a serotype-independent pneumococcal vaccine, the use of highly conserved pneumococcal  
267 protein antigens has become an attractive alternative to achieve immune response against *S. pneumoniae*  
268 [28]. PsaA, a 35-kDa lipoprotein present in all serotypes known to date, is capable of inducing herd

269 immunity against the pathogen [29], and studies of its co-administration with PCV7 have demonstrated to  
270 increase serotype coverage and immunogenicity of PCV7 by reducing nasopharyngeal carriage [30].  
271 In our study, the PsaA was obtained by rDNA technology and subsequently, the free amines present in the  
272 lysine amino acids of the PsaA were derivatized to produce a thiolated protein. The functionalization with  
273 SATA adds sulfhydryl groups to proteins in a protected form. Thus, PsaA when modified with SATA can  
274 be stored for extended time periods and the sulfhydryl groups required for the conjugation reactions will be  
275 exposed by treating with the hydroxylamine. Conjugation reaction between the PsaA protein and the SATA  
276 group is described in **Supplementary Figure 1a**. The MALDI-TOF technique (**Figure 1a**) used to  
277 determine the protein molecular weight showed that the purified PsaA had a mass of 34,059 Da, while  
278 PsaA-SATA conjugated protein had a mass of 35,683 Da. The difference in the molecular weight between  
279 PsaA and PsaA-SATA confirms the successful conjugation of SATA to PsaA antigen in the ratio of 13:1.  
280 The presence of multiple sulfhydryl groups on the protein helps its efficient coupling to the nanocapsules.  
281 Similarly, Derksen et al., have described the use of protein functionalized with SATA for its surface  
282 conjugation to liposomes containing maleimide residues [31]. In addition to this, the sulfhydryl modified  
283 proteins were also used to prepare protein-protein conjugate nanoparticles to enhance the immunogenicity  
284 of the protein antigens [32]. The conformation of the protein antigen is pivotal in conserving the potential  
285 epitopes that are responsible for the immunogenicity [33]. The CD spectra (**Figure 1b**) revealed no changes  
286 in the secondary structural conformation of the PsaA-SATA compared to the existing literature [19]. The  
287 PsaA antigen presented negative peaks at 208 and 221 nm, which were also observed in the conjugated  
288 PsaA-SATA antigen, indicating a similar protein folding pattern of alpha helices and beta sheets in both  
289 cases [19,34].



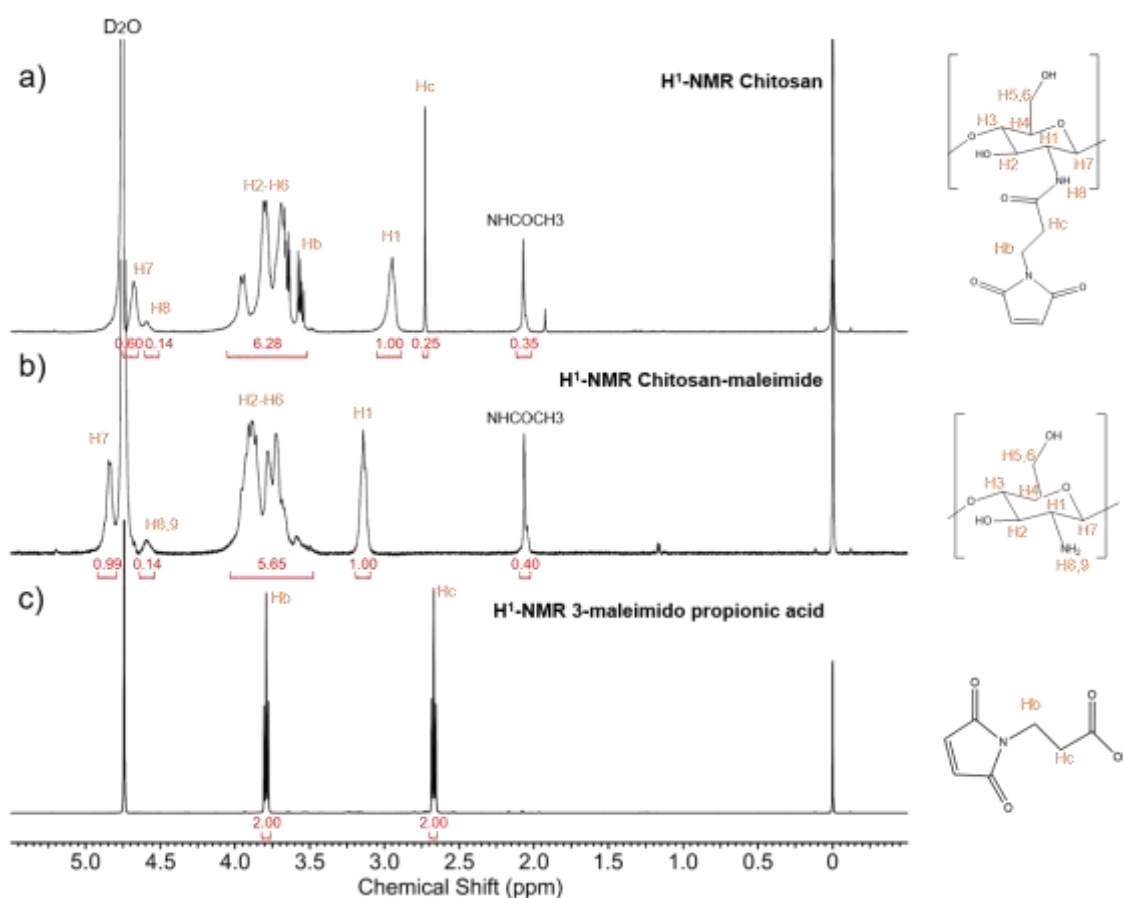
290

291 **Fig. 1:** Pre-formulation characterization of PsaA and its conjugate PsaA-SATA: **(a)** graphs of MALDI-  
 292 TOF for PsaA (blue line) and PsaA-SATA conjugate (green line). **(b)** Overlay of CD spectra for PsaA and  
 293 PsaA-SATA conjugate.

### 294 3.1.2. Chitosan-maleimide conjugation

295 Chitosan is an attractive biomaterial with amine groups for conjugation of ligands [35], and previous studies  
 296 have reported its successful covalent conjugation with maleimide groups [36]. Maleimide selectivity and  
 297 efficient cross-linking with thiol groups, via Michael addition, has allowed the bioconjugation of chitosan  
 298 with biomolecules such as peptides [37] or nucleic acids [38], avoiding the generation of reaction by-  
 299 products. In the present work, conjugation between CS and maleimide propionic acid was performed and  
 300 CS and conjugated CS-maleimide samples were freeze-dried and redispersed in deuterium oxide (D<sub>2</sub>O).  
 301 Conjugation reaction between the polysaccharide and the 3-maleimidopropionic acid group is described in  
 302 **Supplementary Figure 1b**. Their <sup>1</sup>H-NMR spectra had been recorded from 0 to about 10 ppm using a  
 303 proton NMR spectrometer, to confirm the successful conjugation. The typical CS spectrum was confirmed  
 304 in **Figure 2b**, which presented a signal at  $\delta \sim 4.9$ , corresponding to H<sub>7</sub> anomeric proton, the ring proton  
 305 chemical shift (H<sub>2</sub>-H<sub>6</sub>) as overlapping signals at  $\delta \sim 3.6$ -4.0, which confirmed the presence of the

306 glucosamide moiety, while adjacent amino group ring proton ( $H_1$ ) appeared at  $\delta \sim 3.2$ . The methyl group  
 307 of the non-deacetylated part of the polysaccharide was expressed at  $\delta \sim 2.1$  ( $NHCOCH_3$ ), [39], and  
 308 deacetylation degree  $>85\%$  could also be confirmed basis of proton integrals. In **Figure 2a** there still  
 309 appeared signals similar to that native chitosan signals at 2.1 ppm ( $NHCOCH_3$ ), anomeric proton at 2.9 ppm  
 310 ( $H_1$ ) and glucosamide moiety at 3.8-4 ppm ( $H_2$  to  $H_6$ ) [40]. The presence of new peaks Hb and Hc at  $\sim 3.5$   
 311 and 2.7 ppm, respectively, representative of typical protons of the maleimide moiety (**Figure 2c**), were in  
 312 accordance with the chitosan chemical modification, proving the successful attachment of chitosan to  
 313 maleimide propionic acid.



314

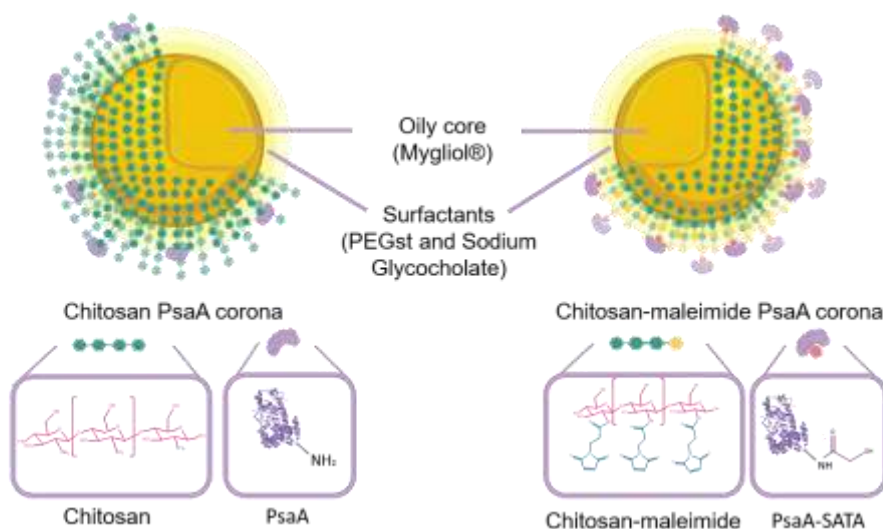
315 **Fig. 2:**  $^1H$ -NMR (400 MHz,  $D_2O$ ) spectra and integration peaks of Chitosan-maleimide (a), Chitosan (b),  
 316 3-maleimidopropionic acid (c), and their respective chemical structures (right). All chemical shifts were  
 317 expressed as  $\delta$  in parts per million (ppm), using the chemical shift of the residual solvent resonances as  
 318 references ( $D_2O$ :  $\delta = 4.80$  ppm).

### 319 3.2. Preparation and physicochemical characterization of chitosan nanocapsules

#### 320 3.2.1. Physicochemical characterization of nanocapsules

321 The combination of antigens with adjuvants into an optimal delivery system is a key for the development  
 322 of a successful vaccine. In addition, aspects such as particle size or surface charge are crucial for the  
 323 interaction and uptake of particles by immune cells [41]. The delivery carrier was selected based on the  
 324 knowledge generated by our group and the protein antigen PsaA was associated on the surface of the  
 325 nanocapsule to obtain a nanovaccine that mimics the pathogen structure and be able to generate a specific  
 326 immune response.

327 CS NCs are made of a hydrophobic oily core surrounded by a hydrophilic coating. This core-corona  
 328 structure uses lipids as core components allowing nanocapsules to interact with and penetrate through  
 329 mucosal surfaces [42]. During the first step, we evaluated different ratios of surfactant:oil (data not shown)  
 330 and the impact on the particle size and polydispersity of the resulting nanoemulsion (NE), and we selected  
 331 nanometric size particles with narrow size distribution to form the oily core of the nanocapsules. The  
 332 amount of Miglyol<sup>®</sup> was the main variable affecting the size of nanocapsules. Similar results were  
 333 previously observed for other polymeric nanocapsule compositions such as those described by González-  
 334 Aramundiz et al [21]. The use of non-ionic surfactants such as PEG-st 40 helps in preventing aggregation  
 335 of particles during the formation of initial NE [43], whilst SGC was used as a co-surfactant that provides  
 336 negative charge and enhanced stability to the oil core of the NCs [44]. As shown in **Figure 3**, chitosan  
 337 molecules were anchored to the surface due to ionic interactions between polymer chains and negatively  
 338 charged oily core, following an ionic interaction procedure, as previously described for chitosan coating  
 339 colloidal systems [45], resulting in a core-coated nanostructure.



340

341 **Fig. 3:** Schematic representation of chitosan polymeric NCs developed in this work. Non-conjugated CS-  
342 antigen nanocapsules (left) and CS-antigen nanocapsules after thiol/maleimide conjugation (right). Design  
343 was created by Biorender® and ChemDraw® graphics programs.

344 NCs were prepared using the solvent displacement technique. As shown in **Table 1**, in all cases, they were  
345 monodisperse with a size range of 245-266 nm and the presence of a CS coating surrounding the oily core  
346 was corroborated by obtaining a positive surface charge of +30 mV, due to the amine groups in the CS  
347 structure. The NCs exhibited an increase in particle size and the surface charge decreased in the presence  
348 of antigen when compared with blank CS NCs. This increase in size could be considered as an indicator of  
349 a successful binding between the protein and the surface CS of the nanocapsules, and it could also be related  
350 to the presence of maleimide-groups as previously described for the development of thiolated-CS liposomes  
351 [46].

### 352 3.2.2. Association efficiency

353 Nanoparticle formulations prepared with thiol-maleimide coupling resulted in higher PsaA association  
354 efficiency than formulations without this covalent modification. Namely, the association efficiency of  
355 protein conjugated to the surface of NCs was approximately 3 times higher with PsaA-SATA compared to  
356 ones where the antigen was associated without polymer-protein conjugation reaction (86% versus 34%,  
357 approximately). Covalently conjugated NCs also preserved their particle integrity and physicochemical  
358 properties, so that they were expected to improve antigen delivery and activation of APCs, enhancing  
359 immunogenicity compared to non-conjugated NCs.

360 For uptake studies, the conjugation of CS-maleimide with Cy5 dye was first performed and nanocapsules  
361 were prepared using the same procedure previously described. The incorporation of the fluorophore did not  
362 alter the NCs original properties.

Formulation name	Size (nm)	Antigen:CS ratio	PDI	Z potential (mV)	Association Efficiency (%)
CS NCs	245 ± 20	-	< 0.1	31 ± 2	-
CS PsaA NCs	248 ± 21	1:5	< 0.1	29 ± 2	34 ± 9
CS-maleimide NCs	252 ± 23	-	< 0.1	31 ± 1	-
CS-maleimide PsaA NCs	266 ± 32	1:5	< 0.2	30 ± 1	86 ± 13
CS-maleimide Cy5 PsaA NCs	254 ± 16	1:5	< 0.1	29 ± 1	-

363

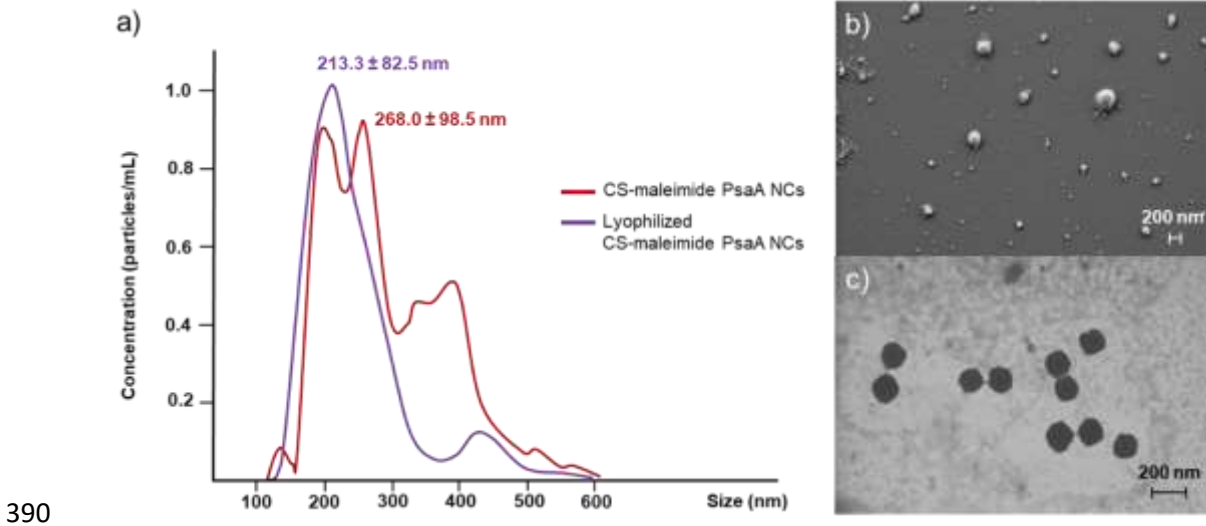
364 **Table 1:** Physicochemical characterization and association efficiency of antigen-conjugated and non-  
365 conjugated NCs. Particle size and polydispersity index were obtained by Dynamic Light Scattering. Data  
366 represent mean ± S.D., n=8. CS: Chitosan; NCs: Nanocapsules; PDI: Polydispersity index.

367 The NTA analysis (**Figure 4a**) of conjugated CS-maleimide PsaA NCs also confirmed previously reported  
368 DLS data showing a particle population of 268 ± 98.5 nm (red line), which corresponds to NCs. Analysis  
369 of the conjugated CS NCs in solution showed that the concentration/size distribution was less homogeneous  
370 than in case of lyophilized NCs, with more than one population of particles. Smaller NCs could be derived  
371 of NTA technique, where a higher dilution of CS-maleimide NCs (1:100) might had occasioned their  
372 rupture [47], while aggregation of primary NCs into large NCs could be consequence of the decrease of  
373 repulsive forces between the particle surfaces after chemical coating modification [48].

374 To assess the stability of conjugated CS-maleimide PsaA NCs after freeze drying process, formulations  
375 were lyophilized in the presence of trehalose 5%. After this procedure, the nanocapsules (purple line) were  
376 easily redispersed in ultrapure water and a slight change (< 50 nm) in the particle diameter was observed  
377 after NTA analysis. It was also observed that a lower concentration of nanocapsules tended to aggregate  
378 after lyophilization procedure compared with NCs in solution, which confirmed trehalose as an appropriate  
379 cryoprotectant to prevent nanoparticle aggregation. Production yield calculated by the difference obtained  
380 between the initial weight and the weight obtained after lyophilization was 67±21%. This freeze-dried  
381 chitosan nanocarrier could preserve their integrity upon storage without compromising its physicochemical  
382 properties, which is a very attractive feature in terms of developing a future thermostable vaccine  
383 formulation [49].

384 3.2.3. Morphological characterization

385 Different microscopic techniques were used to characterize the conjugated NCs. FESEM and STEM  
386 microscopy images revealed a homogeneous population of particles with round-shape structures, which  
387 confirm the spherical structure of the NCs. The average particle physical diameter was around 220 nm that  
388 corroborated the hydrodynamic NCs diameter values obtained by DLS, where slightly higher values were  
389 influenced by the interactions between the particles and the dispersion media (**Fig. 4b and 4c**) [50].

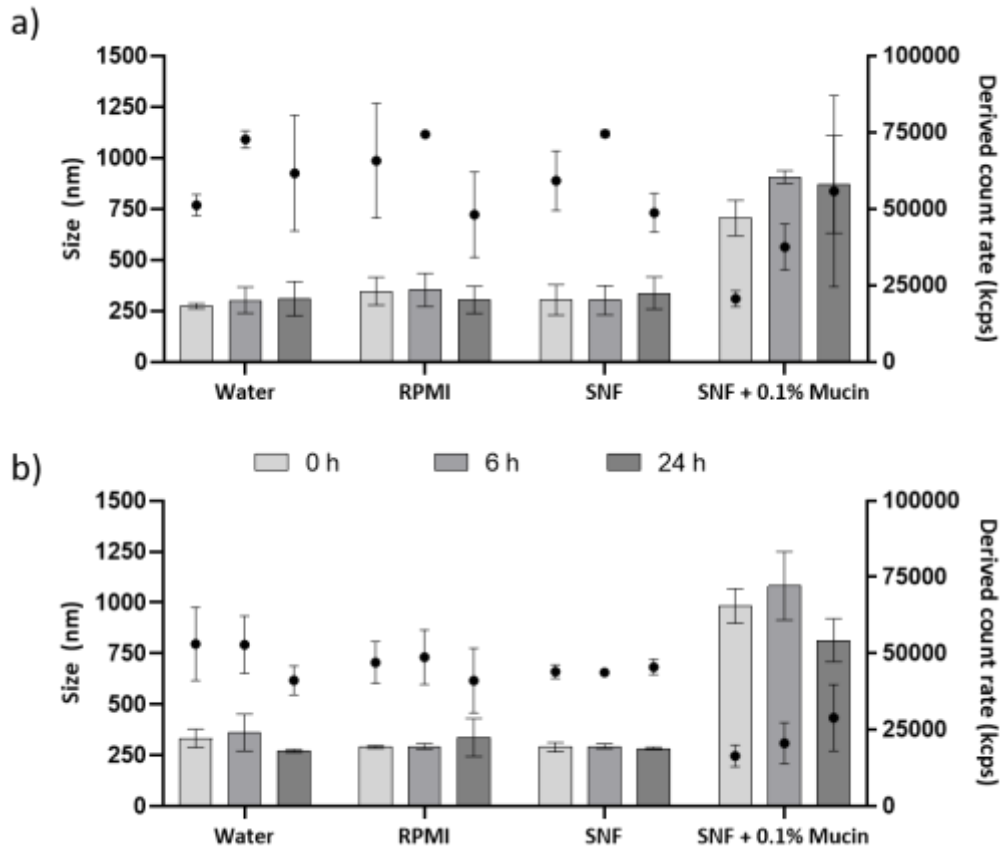


391 **Figure 4:** (a) Representative image of the particles size distribution by Nanoparticle Tracking Analysis of  
392 conjugated nanocapsules in solution (red line) and conjugated nanocapsules resuspended after  
393 lyophilization procedure (purple line), with the mean particle size  $\pm$  standard deviation. Electron  
394 microscopy scanning (b) and transmission (c) images of conjugated Chitosan-maleimide PsaA NCs. Scale  
395 bars are indicated in each image. NCs: Nanocapsules.

396 3.2.4. Colloidal stability

397 Apart from obtaining adequate physicochemical properties, particle stability must be guaranteed for the  
398 developed nanosystems. The understanding of the colloidal stability and aggregation of the nanosystems in  
399 the biological media is important for their rational design. Moreover, the nanoparticle aggregation has  
400 shown to influence the *in vitro* cellular responses. Our studies showed that the size of the CS-maleimide  
401 PsaA NCs remained unchanged and no signs of aggregation were observed during a period of 24 h in both  
402 RPMI-1640 and SNF in suspension (**Figure 5a**), and after the freeze-drying process (**Figure 5b**), which  
403 suggest that the NCs were stable in the biological media and could be further proceeded for primary cell  
404 culture studies. However, there was a considerable increase in particle size when SNF medium was

405 supplemented with mucin type III. This increase in the particle size of the NCs can be attributed to the  
406 decrease in the Brownian motion of the particles due to higher viscosity of the medium in the presence of  
407 mucin, as well as structural properties of CS such as deacetylation degree or molecular weight [51]. This  
408 electrostatic interaction between the positively charged chitosan nanocapsules and the negatively charged  
409 mucin molecules yields protein-polysaccharide complexes [52]. According to Feng et al [53], dynamic  
410 viscosity could be calculated by DLS method, using water viscosity values (~0.89 cP at 25°C) and  
411 commercial polystyrene latex nanoparticles of known size (Magsphere Inc, USA) as reference. Values of  
412 ~1.21 cP for SNF media and ~1.41 cP for SNF media supplemented with mucin type III confirmed this  
413 increase in dynamic viscosity. Conjugated CS-maleimide PsaA NCs became larger and their brownian  
414 movement slower after incubation in SNF with mucin Type III, which might reflect the mucoadhesive  
415 properties of chitosan nanocapsules with mucin macromolecules [54]. Chitosan-mucin interaction by  
416 hydrogen and electrostatic bonding has been shown to be suitable for pharmaceutical and biomedical  
417 applications in the oral, nasal or ocular routes [55]. However, future in vivo experiments will be needed to  
418 confirm the mucoadhesive properties of CS-PsaA nanocapsules conjugated for nasal application. In  
419 addition, all formulations have maintained constant stability profiles in aqueous suspension at 4 °C for at  
420 least, 1 month (**Supplementary Figure 2**).



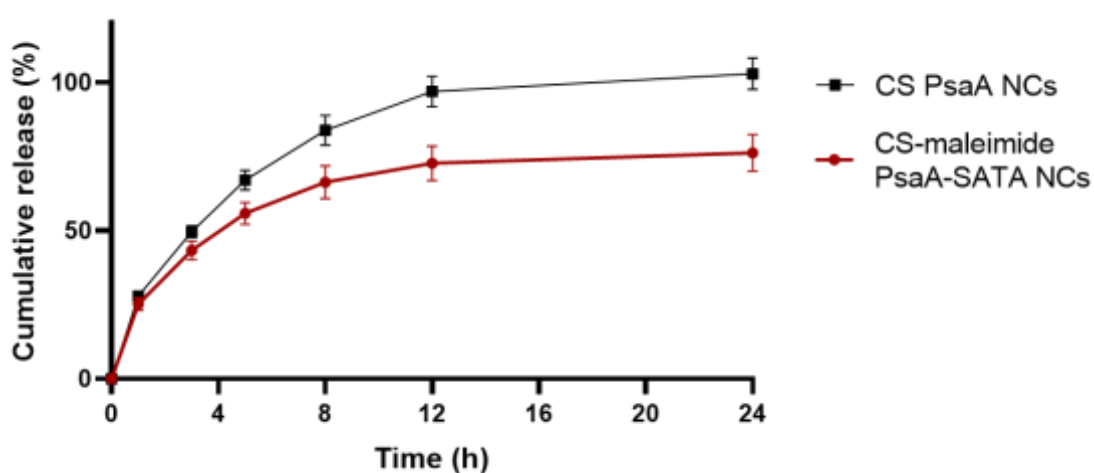
421

422 **Fig. 5:** Stability of conjugated CS-maleimide PsaA NCs in suspension (a) and lyophilized (b) conditions  
 423 in water, cellular media (RPMI), simulated nasal fluid alone (SNF) and with mucine type III (SNF+ 0.1%  
 424 Mucin). Bars represent size (nm), and dots represent derived count rate (kcps) (mean± SD; n=3).

425 **3.3. Release studies**

426 The *in vitro* release behavior of PsaA from CS NCs was investigated using simulated nasal fluid (SNF pH  
 427 = 6.5). The accumulative release study of non-conjugated CS-PsaA and conjugated CS-maleimide PsaA  
 428 NCs was carried out after 24 h of nanocapsules incubation in SNF by analyzing the total amount of free  
 429 protein in the media at each time point. Total loading was estimated considering the previously reported  
 430 association efficiency rates achieved after physical (CS-PsaA NCs) and chemical (CS-maleimide PsaA  
 431 NCs) conjugation. Values of protein released over time were obtained by extrapolation with a BSA protein  
 432 concentration range in SNF. As observed in **Figure 6**, NCs presented an initial fast release during the first  
 433 3 hours of approximately the half of the PsaA antigen from the formulations to the medium. The release  
 434 experiment indicated that the protein was gradually released from the nanocapsules in a time-dependent  
 435 manner, and that this antigen release remained stable after 8 h. However, a sustained antigen release pattern

436 was observed after 3 hours in the CS-PsaA NCs, reaching values of 100% of the release at 24 h, contrary  
437 to the CS-maleimide NCs, where the release was slowed down, reaching values over 76% at 24 h. The  
438 relatively slower and sustained release in conjugated CS-maleimide PsaA formulation may be ascribed to  
439 the chemical conjugation which produced a stronger interaction between the antigen and the  
440 polysaccharide. As showed in similar studies in maleimide-bearing nanogels [56] and maleimide-  
441 functionalized PEGylated liposomes [57], carrier capacity to retain and release the drug was sustained for  
442 a prolonged time-period. Overall, both conjugated and free antigen release presented a biphasic profile with  
443 a faster initial release followed by a second phase with slow and delayed tendency release profile.



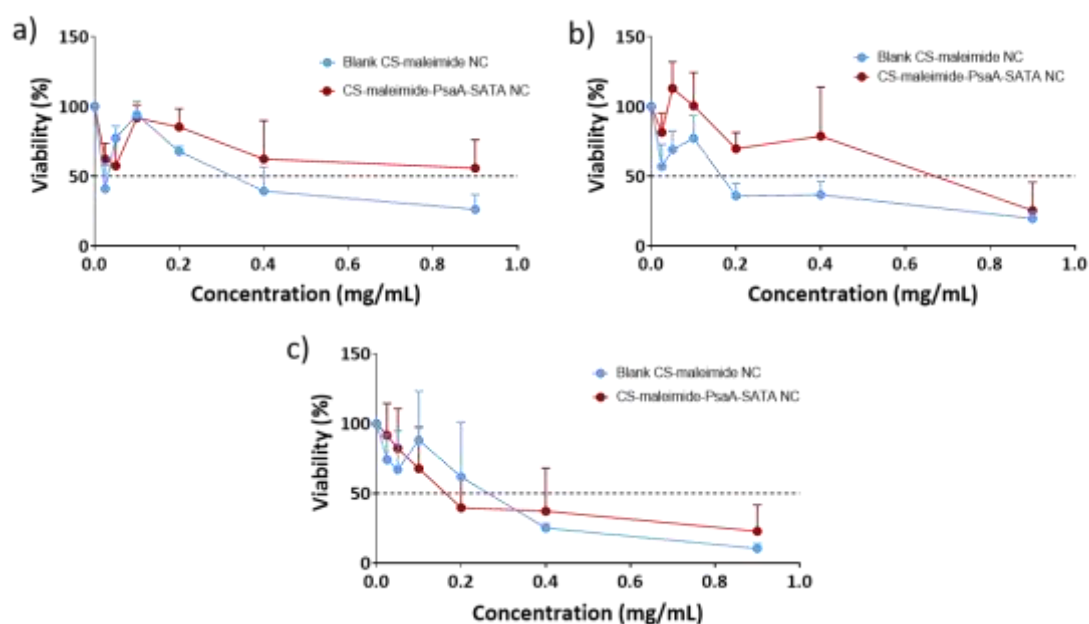
444

445 **Fig. 6:** *In vitro* cumulative release profile of PsaA antigen from chitosan PsaA and chitosan-maleimide  
446 PsaA NCs (mean± S.D.; n=6). CS: Chitosan, NCs: Nanocapsules.

#### 447 3.4. NCs toxicity on immune cells

448 To investigate the biocompatibility of both types of conjugated CS-maleimide nanocapsules (blank and  
449 antigen loaded), an *in vitro* MTS assay was performed to study the influence of the nanocapsules on the  
450 metabolic activity of macrophages and DCs. Since cationic nanoparticles generally have better electrostatic  
451 attractions with the negatively charged cell surface, their toxicity also might increase [58]. After 4 h (**Figure**  
452 **7a**) and 24 h (**Figure 7b**) of CS-maleimide and CS-maleimide PsaA NCs incubation with macrophage Raw  
453 264.7 cells, MTS assay showed a significant reduction in cell viability (mitochondrial reductase activity)  
454 at concentrations > 200 µg/mL. Membrane damage was more pronounced in blank CS-maleimide NCs,  
455 being practically total at values of 800 µg/mL, while in the case of protein-conjugated nanocapsules it  
456 remained around 40% at higher doses. Similar effects on toxicity were observed after incubation of NCs

457 with iDCs for 24 h (**Figure 7c**), although in this case, toxicity was apparently higher in blank CS-maleimide  
 458 NCs.  
 459 In a second instance, cell toxicity values were also verified *via* 7-AAD cytotoxicity assay test at 24 h.  
 460 Considering that dendritic cells with compromised membranes were stained with 7-AAD, untreated cells  
 461 were use as control for viable cells. The flow cytometry analyses performed (**Supplementary Figure 3**)  
 462 showed a decrease in the number of viable cells as the CS-maleimide PsaA NCs concentration increased,  
 463 reaching dendritic cell viability values of 65% at NCs concentrations of 900  $\mu\text{g/mL}$ .



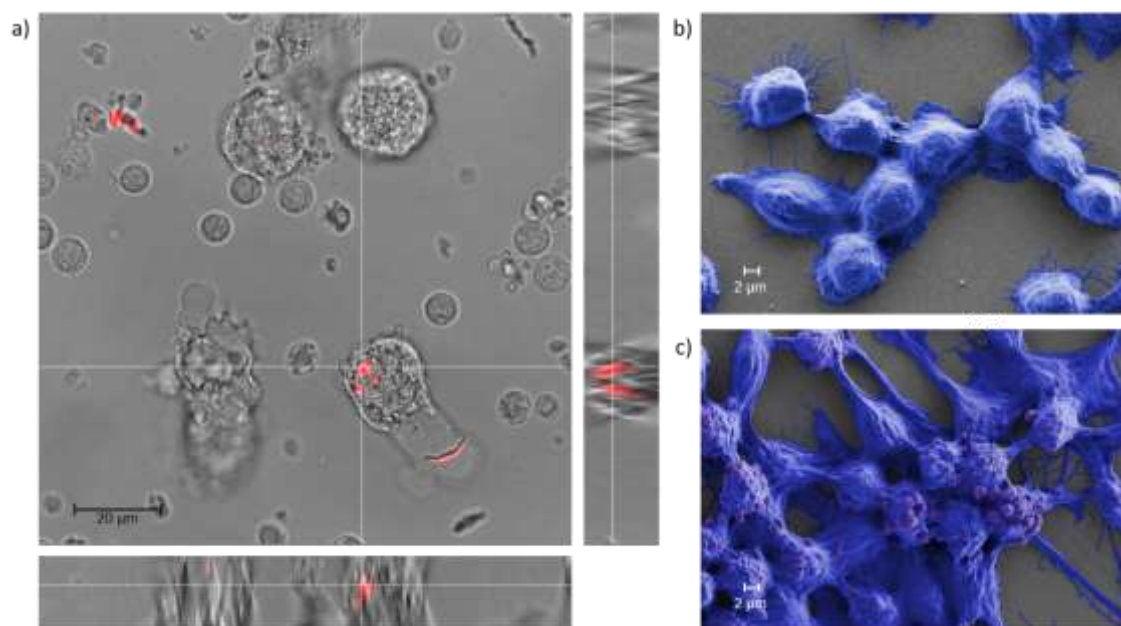
464

465 **Fig. 7:** Effect of CS-maleimide and CS-maleimide PsaA NCs on the viability of Raw 264.7 macrophages  
 466 (**a, b**) and immature dendritic cells (**c**). MTS assay performed on Raw 264.7 cell lines incubated with either  
 467 CS-maleimide (blue lines) or CS-maleimide PsaA (red lines) NCs using different concentrations of  
 468 nanocapsules during (**a**) 4 h and (**b**) 24 h. (**c**) MTS assay performed on iDCs after incubating them with  
 469 different concentrations of nanocapsules for 24 h. Results were normalized with the percentage of live iDCs  
 470 incubated in culture media alone and dead iDCs incubated with Triton (5%, 1x) (mean  $\pm$  S.D; n=4). CS:  
 471 Chitosan; NCs: Nanocapsules.

### 472 3.5. Interaction of NCs with immune cells

473 Immune cells are able to capture antigens in many different ways, such as phagocytosis, macropinocytosis,  
 474 or by expressing surface receptors causing endocytosis [59]. Once the antigen has been captured by the  
 475 antigen presenting cells, it is processed and presented on the cell surface by Major Histocompatibility

476 Complex (MHC) [60]. To confirm whether our nanocarriers were able to interact with such immune cells,  
477 we examined the efficacy of CS-maleimide PsaA NCs on antigen uptake in primary cultures of human  
478 monocyte-derived iDCs and in the macrophage Raw 264.7 cell line. After incubating the Cy5-labelled NCs  
479 (both blank and antigen loaded), the presence of intracellular fluorescence due to the Cy5-labelled NCs  
480 confirmed the internalization of the nanocapsules by the DCs. The images obtained from the confocal  
481 scanning microscopy confirmed that the nanocapsules (top **Figure 8a**, red channel) were located within the  
482 dendritic cells (bottom, contrast microscope DiC channel) and intracellular distribution of CS-maleimide  
483 NCs could be seen throughout the different sections of dendritic cells (**also see online video resource in**  
484 **Supplementary material**). The physical appearance of DCs could also provide information about their  
485 maturation and activation status, for example, by the formation of their characteristic dendrites as seen in  
486 our case [25].  
487 On the other hand, the interaction of macrophages with nanocapsules was analyzed by FESEM microscopy.  
488 The presence of protrusions on the surface of cells observed in FESEM images (**Figure 8c**) suggested a  
489 possible grouping of nanocapsules and recognition by macrophages.



490

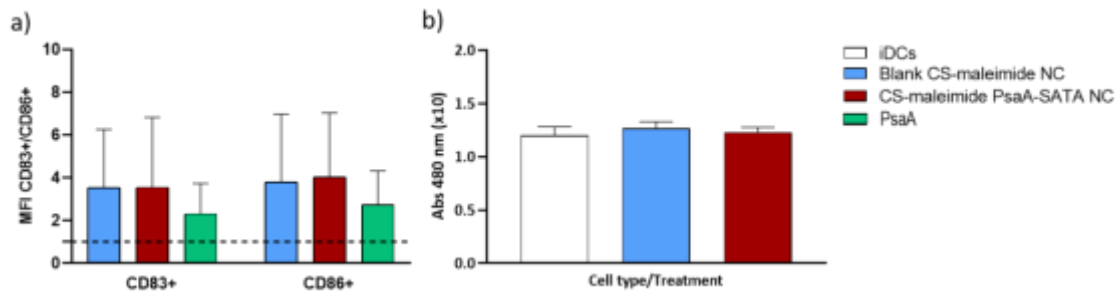
491 **Fig. 8:** CLSM images of Cy5-labelled CS-maleimide PsaA NCs incubated with DCs (**a**) and FESEM  
492 images of Raw 264.7 cells alone (**b**) and after incubation with CS-maleimide PsaA NCs (**c**). Raw 264.7  
493 cells (blue), and nanocapsules (purple, indicated with white arrows) in (b) and (c) were artificially colored  
494 to ease their visualization.

### 495 3.6. Human DCs phenotype analysis

496 To evaluate the effect that NCs may have on iDC phenotype, the expression of T lymphocyte costimulatory  
497 molecules CD83 and CD86 (indicators of pro-inflammatory activated phenotype in dendritic cells) were  
498 analyzed by flow cytometry. The co-stimulatory marker CD86 designates to be a marker primary DCs  
499 maturation expressed within first 24 h and interacts with the CD28 for the T cell activation, while the  
500 increased CD83 is observed in mature/activated DCs. Several studies have proven that antigen delivery to  
501 DCs upregulates expression of both CD83 and CD86 that are known to induce T cell receptor signalling  
502 and promote T cell activation [61]. In our study, both the blank and antigen loaded CS-maleimide NCs  
503 showed an increase in the expression of these maturation markers. The expression of CD83 and CD86  
504 (**Figure 9a**) were 4 folds higher in the case of DCs primed with blank and antigen loaded CS-maleimide  
505 NCs when compared to iDCs (MFI=1). However, iDCs treated with PsaA alone displayed a 2 and 3-fold  
506 lower expression of CD83 and CD86 markers, respectively. Overall, the results suggest that either the blank  
507 or antigen loaded NCs can upregulate the co-stimulatory markers in comparison to the antigen alone.

### 508 3.7. NCs tolerogenic effect on immature DCs

509 Antigen-presenting cells such as iDCs play an important role in immune regulation, not only as inductors  
510 but also inhibitors of an immune response. 2,3-Indoleamine dioxygenase (IDO) is an enzyme involved in  
511 tryptophan catabolism, essential for the growth of microorganisms, which regulates T-cell tolerance [62].  
512 IDO is a potent immune-suppressive enzyme in macrophages and dendritic cells whose physiological  
513 function is to catabolize the essential amino acid tryptophan into the stable metabolite, kynurenine which  
514 is known to induce the apoptosis of Th1 cells *in vitro* [63]. In addition, it is known that the IDO expression  
515 by the DCs can greatly impact peripheral tolerance and immune regulation. In this line, we performed a  
516 study to evaluate if the NCs formulations were inducing a tolerogenic phenotype on iDCs in terms of T-  
517 cell suppression and tolerance promotion (opposite to a pro-inflammatory response), by quantifying the  
518 IDO enzymatic activity after iDCs treatment with NCs. The results obtained from our study showed that  
519 the response in the DCs treated with either blank or antigen loaded CS-maleimide NCs signal was similar  
520 to one observed in iDCs (**Figure 9b**), indicating no tolerogenic effect of the NCs.



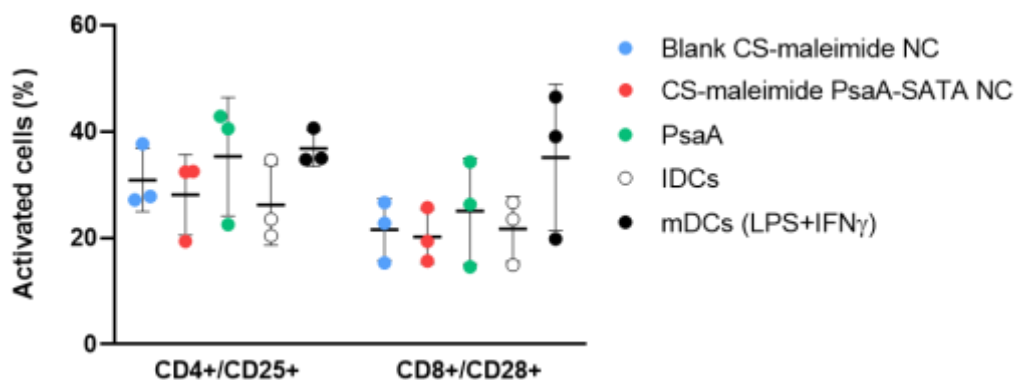
521

522 **Fig. 9:** (a) Quantification (%) of the expression of iDC maturation markers CD83 and CD86. Results are  
 523 expressed as the ratio between the markers mean fluorescence intensity (MFI) in iDCs incubated with the  
 524 different NCs and the MFI of iDC incubated in culture media alone (MFI=1). The dotted line corresponds  
 525 to the signal from the iDCs. (b) Indoleamine 2,3-dioxygenase (IDO) activity in dendritic cell cultures. iDCs:  
 526 immature dendritic cells; CS: Chitosan; NCs: Nanocapsules) (mean  $\pm$  SEM; n=3 donors).

### 527 3.8. Activation CD4 and CD8 T cells by NCs

528 Stimulation of antigen specific CD4+ and CD8+ T lymphocytes is essential for efficient adaptive immunity.  
 529 Therefore, we have assessed the ability of the DCs pulsed with antigen, blank CS-maleimide NCs or CS-  
 530 maleimide PsaA NCs to activate T lymphocytes. The effect of conjugated NCs on the activation of T  
 531 lymphocytes in an allogenic response was analyzed by flow cytometry. Blank CS-maleimide, CS-  
 532 maleimide PsaA NCs (150  $\mu$ g/mL) and PsaA antigen alone were incubated with iDCs and then, the  
 533 capability of this NC-incubated iDCs to activate allogenic lymphocytes was analyzed quantifying the  
 534 expression levels of CD25 (for CD4 T lymphocytes) and CD28 (for CD8 T lymphocytes). As shown in  
 535 **Figure 10**, mature DCs (mDCs) showed a greater capacity of activating both CD4 and CD8 T lymphocytes  
 536 (black dots) than iDCs (open dots). On the other hand, preincubation of the iDCs with PsaA protein (green  
 537 dots), blank CS-maleimide NCs (blue dots), and CS-maleimide PsaA NCs (red dots), induced similar  
 538 percentages of activated CD4 and CD8 T lymphocytes when compared to iDCs.

539 In all cases, incubation of iDCs in the presence of NCs caused these APCs to have a similar capacity to  
 540 stimulate CD4 and CD8 lymphocytes to iDCs, and were lower compared to mDCs. Also, levels of both  
 541 activated CD4+CD25+ and CD8+CD28+ CD4 T cells were similar for loaded and non-loaded  
 542 nanocapsules. However, no significant differences were found between treatments, probably due to donor  
 543 variability. The similar values between both treatments on the effect of T cell activation could be a  
 544 consequence of the composition of the nanocapsules, rather than the presence of the antigen on the surface.  
 545 [64].



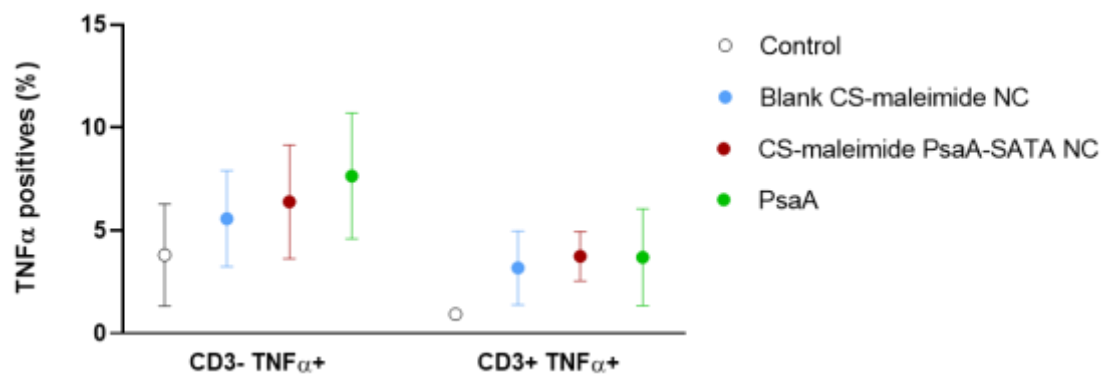
546

547 **Fig. 10:** Percentages (%) of activated T cells after iDCs incubation with formulations. Non-treated iDCs  
 548 and LPS and IFN $\gamma$  treated iDCs (mDCs) were used as controls (mean  $\pm$  SEM; n=3 donors, 2-way ANOVA  
 549 test). CS: Chitosan; iDCs: immature Dendritic Cells; mDCs: mature Dendritic Cells; NCs: Nanocapsules.

### 550 3.9. Cytokine secretion by PBMCs incubated with different NCs.

551 In the process of developing a powerful immune response, dendritic cells capture antigens thanks to pattern  
 552 recognition receptors (PRRs), leading to phenotypic and maturation changes [65]. Depending on the  
 553 alterations they undergo and the co-stimulation molecules they express, different responses will take place  
 554 from the T cells (Th1, Th2 or Th17) [66]. The secretion of cytokines by Th1 CD4+ cells (such as IL-2,  
 555 IFN $\gamma$ , IL-10 or TNF $\alpha$ ) is necessary in order to achieve protection against pneumococcal infection [2].  
 556 TNF $\alpha$ , secreted by either macrophages, monocytes or activated lymphocytes acts as an inflammatory  
 557 marker and protects against the infectious pathogens. TNF $\alpha$  production can activate the T cells or can be a  
 558 product of the activated T cells. In this procedure, we quantified by intracellular cytokine staining the  
 559 production of TNF $\alpha$  by T lymphocytes (CD3+) and non-T cells (CD3-) after incubation with NCs. As can  
 560 be seen in **Figure 11**, TNF $\alpha$  production was higher in the CD3- (monocytes) population, being around 5-  
 561 8% compared to CD3+ (lymphocytes) population, where it did not exceed a 5% in any case. In both cases,  
 562 a higher percentage of TNF $\alpha$ -positive cells was seen after incubated with the different NCs and the PsaA  
 563 protein compared to iDCs, especially for the CD3+ T cells. Although no statistical differences were found  
 564 in the different treatments due to the high variability among donors, the obtention of slightly higher cytokine  
 565 secretion levels in CS-maleimide PsaA NCs could be a consequence of the presence of PsaA attached on  
 566 their surface. These results were in agreement with previous studies evaluating the effect of cationic CS  
 567 NCs in inducing inflammatory responses, where cytokine levels were remarkable in one out of three donors  
 568 tested [67]. Likewise, when the PsaA protein was used, a clear increase in the percentage of TNF $\alpha$ -positive

569 cells was observed when compared to control cultures. This may indicate the external presence of the  
570 bacterial endotoxin lipopolysaccharide LPS, a potent activator of innate immunity.



571

572 **Fig. 11:** Percentages (%) of TNFα positive cells (CD3+ and CD3-) after treatment with CS-maleimide NCs,  
573 antigen loaded CS-maleimide PsaA NCs and PsaA antigen alone (mean ± SEM; n=3 donors, 2-way  
574 ANOVA test). CS: Chitosan; NCs: Nanocapsules.

#### 575 4. Conclusion

576 In the design of targeted nanovaccines towards nasal immune cells, a specific nanocarrier design with  
577 mucoadhesive properties is crucial to achieve a higher residence time, avoiding mucociliary clearance and  
578 crossing nasal epithelium. In this work, combination of the antigenic protein membrane PsaA together with  
579 the high capacity of drug association of chitosan-maleimide modified nanocapsules has been positioned as  
580 an interesting perspective for *Streptococcus pneumoniae* vaccination. Results supported the versatility of  
581 non-capsular pneumococcal antigens as vaccine candidates for an efficient mucosal administration.  
582 Developed nanocapsules presented a high effective payload of antigen after covalent thiol linkage,  
583 mucoadhesiveness together with high physical and biological stability. The nanocapsules capacity to  
584 interact with immune cells was conserved and enhanced compared to the free antigen, suggesting them a  
585 “green light” future serotype-independent pneumococcal vaccine candidate. To further assess the ability of  
586 these nanocapsules as vaccine delivery systems, the evaluation of antigen-specific responses and cytokine  
587 profiles is currently under way.

#### 588 Acknowledgment & Funding

589 This work was supported by ‘Ministerio de Economía y Competitividad’ – (RETOS - SAF2016-79230-R -  
590 ERC2018-092841 and PID2019-108727RB-I00). Sandra Robla acknowledges the financial support from

591 the Xunta de Galicia (Centro Singular de Investigación de Galicia accreditation 2019-2022) and the  
592 European Union (European Regional Development Fund - ERDF), code ED431G 2019/02. Maruthi  
593 Prasanna acknowledges his doctoral fellowship from the European Commission, Education, Audiovisual  
594 and Culture Executive Agency (EACEA), under the Erasmus Mundus program, “NanoFar: European  
595 Doctorate in Nanomedicine and Pharmaceutical Innovation” (Project: 2015-01-C4). The authors have no  
596 other relevant affiliations or financial involvement with any organization or entity with a financial interest  
597 in or financial conflict with the subject matter or materials discussed in the manuscript apart from those  
598 disclosed.

#### 599 **Conflicts of interest/Competing interests**

600 Authors declare that they have no conflict of interest.

#### 601 **Ethics approval**

602 All procedures followed were in accordance with the ethical standards of the responsible institutional and  
603 national committees on human experimentation and with the Declaration of Helsinki. Informed consent  
604 was obtained from all patients for being included in the study.

#### 605 **Consent to participate**

606 All institutional and national guidelines for the obtention and use of human blood were followed. Blood  
607 was drawn with the informed consent of all subjects and appropriate permission was obtained from the  
608 Institutional Ethics Committee (Comité Ético de Investigación Clínica de Galicia, CEIC).

609 No animal or human studies were carried out by the authors for this article.

#### 610 **Consent for publication**

611 Not applicable

#### 612 **Availability of data and material**

613 Not applicable

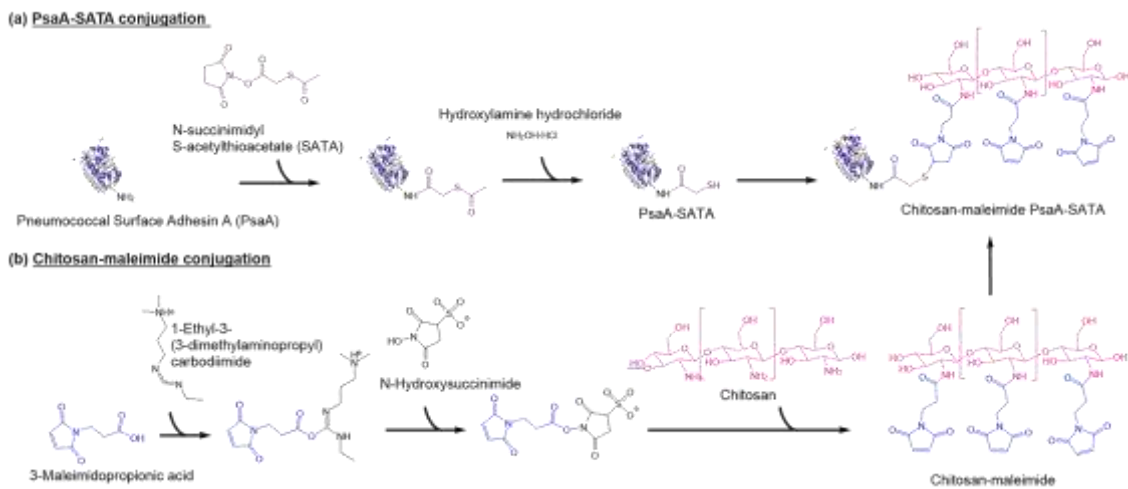
#### 614 **Code availability**

615 Not applicable

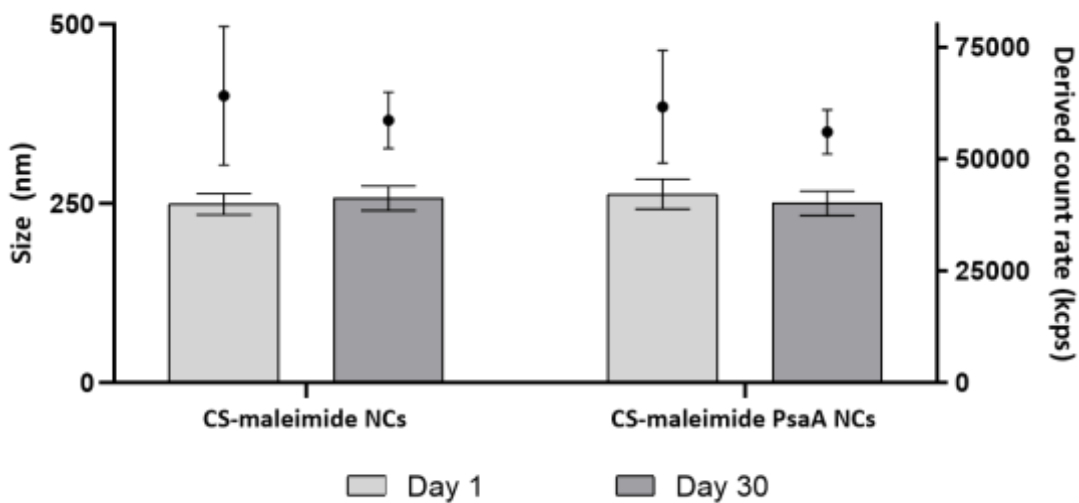
#### 616 **Authors' contributions**

617 Sandra Robla was in charge of the overall experimental execution, data analysis, writing and figure  
 618 preparation. Maruthi Prasanna contributed to the experimental execution and writing. Cyrille Grandjean  
 619 was involved in the synthesis and characterization of the PsaA antigen, reviewing and editing the  
 620 manuscript. R Varela-Calvino was involved in the design and supervision of the in vitro cell experiments,  
 621 reviewing and editing the manuscript. Noemi Csaba was involved in writing, reviewing, editing,  
 622 supervision, project design and administration.

623 **Supplementary material**

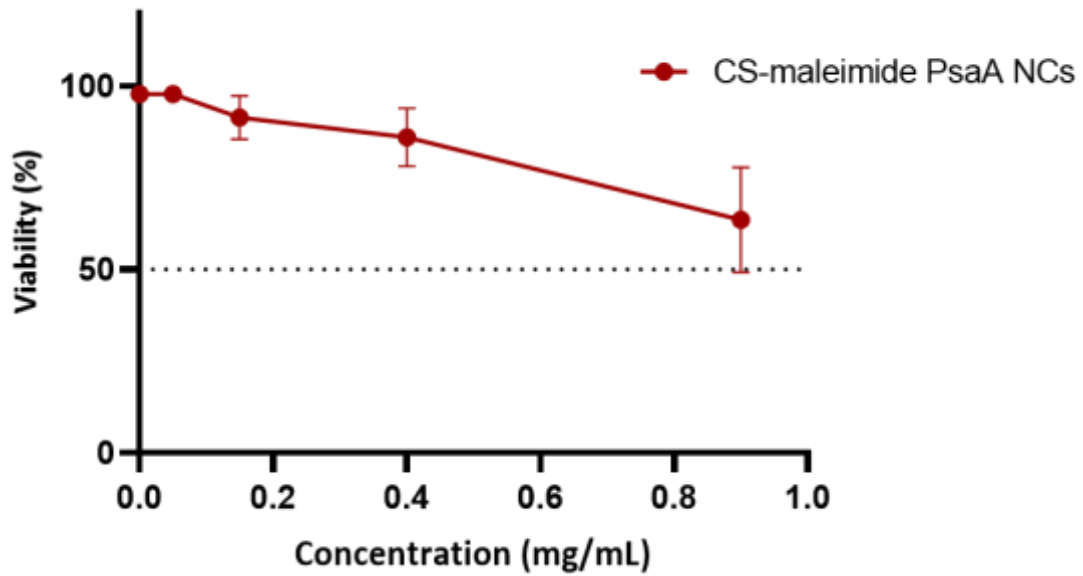


624  
 625 Supplementary Figure 1: (a) Chemical conjugation scheme between PsaA and N-succinimidyl S-  
 626 acetylthioacetate (SATA) group and (b) Chitosan and 3-maleimidopropionic acid group. Reaction synthesis  
 627 yield after purification and lyophilization procedure was ~ 30% and 50%, respectively.



628  
 629 Supplementary Figure 2: Stability of conjugated CS-maleimide PsaA NCs after 1 month under storage

630 conditions (dark and 4°C). Bars represent size (nm), and dots represent derived count rate (kcps) (mean±  
631 SD; n=6). CS: Chitosan; NCs: Nanocapsules.



632

633 Supplementary Figure 3: 7-AAD cytotoxicity study in function of the concentration of the conjugated CS-  
634 maleimide PsaA NCs. (mean± SD; n=3). CS: Chitosan; NCs: Nanocapsules.

635 Online resource 1: Intracellular distribution of Cy5-labelled CS-maleimide PsaA NCs throughout the  
636 different sections of DCs after confocal microscopy.

637 **References**

- 638 1. Pérez-Dorado I, Galan-Bartual S, Hermoso JA. Pneumococcal surface proteins: When the whole is  
639 greater than the sum of its parts. *Mol Oral Microbiol.* 2012;27:221–45.
- 640 2. Singh R, Gupta P, Sharma PK, Ades EW, Hollingshead SK, Singh S, et al. Prediction and  
641 characterization of helper T-cell epitopes from pneumococcal surface adhesin A. *Immunology.*  
642 2014;141:514–30.
- 643 3. Mohammadzadeh M, Mamishi S, Pourakbari B, Mahmoudi S. Recent approaches in whole cell  
644 pneumococcal vaccine development : a review study. 2017;9:381–8.
- 645 4. Leites A, Paula A, Argondizzo C, Esteves S, Jessouron E, Galler R, et al. Cloning and optimization of  
646 induction conditions for mature PsaA ( pneumococcal surface adhesin A ) expression in *Escherichia coli*  
647 and recombinant protein stability during long-term storage. *Protein Expr Purif. Elsevier Inc.;* 2011;78:38–  
648 47.
- 649 5. Bartual SG, Alcorlo M, Martínez-Caballero S, Molina R, Hermoso JA. Three-dimensional structures of  
650 Lipoproteins from *Streptococcus pneumoniae* and *Staphylococcus aureus*. *Int J Med Microbiol. Elsevier;*  
651 2017;1–13.
- 652 6. Rajam G, Anderton JM, Carlone GM, Sampson JS, Ades EW. Pneumococcal surface adhesin A  
653 (PsaA): A review. *Crit Rev Microbiol.* 2008;34:163–73.
- 654 7. Zheng Z, Diaz-Arévalo D, Guan H, Zeng M. Noninvasive vaccination against infectious diseases. *Hum*  
655 *Vaccines Immunother.* 2018;14:1717–33.
- 656 8. Almeida\* AJ, Florindo HF. Chapter 3.1. Nanocarriers Overcoming the Nasal Barriers: Physiological  
657 Considerations and Mechanistic Issues. 2012. p. 117–32.
- 658 9. Calvo P, Remuñan-López C, Vila-Jato JL AM. Chitosan and chitosan/ethylene oxide-propylene oxide  
659 block copolymer nanoparticles as novel carriers for proteins and vaccines. *Pharm Res.;*
- 660 10. Csaba N, Garcia-Fuentes M, Alonso MJ. Nanoparticles for nasal vaccination. *Adv Drug Deliv Rev.*  
661 *Elsevier B.V.;* 2009;61:140–57.
- 662 11. Illum L. Nasal drug delivery - Possibilities, problems and solutions. *J Control Release.* 2003;87:187–  
663 98.

- 664 12. Slütter B, Hagens N, Jiskoot W. Rational design of nasal vaccines. *J Drug Target.* 2008;16:1–17.
- 665 13. Lewis KL, Reizis B. Dendritic cells: Arbiters of immunity and immunological tolerance. *Cold Spring*  
666 *Harb Perspect Biol.* 2012;4.
- 667 14. Cole J, Aberdein J, Jubrail J, Dockrell DH. The Role of Macrophages in the Innate Immune Response  
668 to *Streptococcus pneumoniae* and *Staphylococcus aureus*. *Adv Microb Physiol.* 1st ed. Elsevier Ltd.;  
669 2014. p. 125–202.
- 670 15. Prego C, Torres D, Alonso MJ. The potential of chitosan for the oral administration of peptides.  
671 *Expert Opin Drug Deliv.* 2005;2:843–54.
- 672 16. Prego C, Torres D, Alonso MJ. Chitosan nanocapsules: A new carrier for nasal peptide delivery. *J*  
673 *Drug Deliv Sci Technol.* Elsevier Masson SAS; 2006;16:331–7.
- 674 17. Kean T, Thanou M. Biodegradation, biodistribution and toxicity of chitosan. *Adv Drug Deliv Rev.*  
675 Elsevier B.V.; 2010;62:3–11.
- 676 18. Shi GN, Zhang CN, Xu R, Niu JF, Song HJ, Zhang XY, et al. Enhanced antitumor immunity by  
677 targeting dendritic cells with tumor cell lysate-loaded chitosan nanoparticles vaccine. *Biomaterials.*  
678 Elsevier Ltd; 2017;113:191–202.
- 679 19. Prasanna M, Soulard D, Camberlein E, Ruffier N, Lambert A, Trottein F, et al. Semisynthetic  
680 glycoconjugate based on dual role protein/PsaA as a pneumococcal vaccine. *Eur J Pharm Sci.* Elsevier;  
681 2019;129:31–41.
- 682 20. Grenha A. Chitosan nanoparticles: A survey of preparation methods. *J Drug Target.* 2012;20:291–  
683 300.
- 684 21. González-Aramundiz JV, Presas E, Dalmau-Mena I, Martínez-Pulgarín S, Alonso C, Escribano JM, et  
685 al. Rational design of protamine nanocapsules as antigen delivery carriers. *J Control Release.* Elsevier  
686 B.V.; 2017;245:62–9.
- 687 22. Shen J, Burgess DJ. In vitro dissolution testing strategies for nanoparticulate drug delivery systems:  
688 recent developments and challenges. *Drug Deliv Transl Res.* 2013;3:409–15.
- 689 23. Posch W, Lass-Flörl C, Wilflingseder D. Generation of human monocyte-derived dendritic cells from  
690 whole blood. *J Vis Exp.* 2016;2016:2–7.

- 691 24. Banchereau J, Briere F, Caux C, Davoust J, Lebecque S, Liu Y, et al. Immunobiology of Dendritic  
692 Cells. *Annu Rev Immunol.* 2000;18:767–811.
- 693 25. Kowalewicz-Kulbat M, Ograczyk E, Krawczyk K, Rudnicka W, Fol M. Type of monocyte  
694 immunomagnetic separation affects the morphology of monocyte-derived dendritic cells, as investigated  
695 by scanning electron microscopy. *J Immunol Methods.* Elsevier B.V.; 2016;439:79–82.
- 696 26. Hu X, Zheng W, Wang L, Wan N, Wang B, Li W, et al. The detailed analysis of the changes of  
697 murine dendritic cells (DCs) induced by thymic peptide: Pidotimod(PTD). *Hum Vaccines Immunother.*  
698 2012;8:1250–8.
- 699 27. Lecoœur H, De Oliveira-Pinto LM, Gougeon ML. Multiparametric flow cytometric analysis of  
700 biochemical and functional events associated with apoptosis and oncosis using the 7-aminoactinomycin D  
701 assay. *J Immunol Methods.* 2002;265:81–96.
- 702 28. Moffitt K, Malley R. Rationale and prospects for novel pneumococcal vaccines. *Hum Vaccines*  
703 *Immunother.* 2016;12:383–92.
- 704 29. Tai SS. Streptococcus pneumoniae protein vaccine candidates: Properties, activities and animal  
705 studies. *Crit Rev Microbiol.* 2006;32:139–53.
- 706 30. Whaley MJ, Sampson JS, Johnson SE, Rajam G, Stinson-Parks A, Holder P, et al. Concomitant  
707 administration of recombinant PsaA and PCV7 reduces Streptococcus pneumoniae serotype 19A  
708 colonization in a murine model. *Vaccine.* Elsevier Ltd; 2010;28:3071–5.
- 709 31. Derksen JTP, Scherphof GL. An improved method for the covalent coupling of proteins to liposomes.  
710 *BBA - Biomembr.* 1985;814:151–5.
- 711 32. Scaria P V., Chen B, Rowe CG, Jones DS, Barnafo E, Fischer ER, et al. Protein-protein conjugate  
712 nanoparticles for malaria antigen delivery and enhanced immunogenicity. *PLoS One.* 2017;12:1–19.
- 713 33. Singh R, Gupta P, Sharma PK, Ades EW, Hollingshead SK, Singh S, et al. Prediction and  
714 characterization of helper T-cell epitopes from pneumococcal surface adhesin A. *Immunology.*  
715 2014;141:514–30.
- 716 34. Couñago RM, Ween MP, Begg SL, Bajaj M, Zuegg J, O'Mara ML, et al. Imperfect coordination  
717 chemistry facilitates metal ion release in the Psa permease. *Nat Chem Biol.* Nature Publishing Group;

718 2014;10:35–41.

719 35. Sahoo D, Sahoo S, Mohanty P, Sasmal S, Nayak PL. Chitosan: A new versatile bio-polymer for  
720 various applications. *Des Monomers Polym.* 2009;12:377–404.

721 36. Matsumoto M, Udomsinprasert W, Laengee P, Honsawek S, Patarakul K, Chirachanchai S. A Water-  
722 Based Chitosan-Maleimide Precursor for Bioconjugation: An Example of a Rapid Pathway for an In Situ  
723 Injectable Adhesive Gel. *Macromol Rapid Commun.* 2016;37:1618–22.

724 37. Martínez-Jothar L, Doulkeridou S, Schiffelers RM, Sastre Torano J, Oliveira S, van Nostrum CF, et  
725 al. Insights into maleimide-thiol conjugation chemistry: Conditions for efficient surface functionalization  
726 of nanoparticles for receptor targeting. *J Control Release.* Elsevier B.V; 2018;282:101–9.

727 38. Malhotra M, Tomaro-Duchesneau C, Saha S, Kahouli I, Prakash S. Development and characterization  
728 of chitosan-PEG-TAT nanoparticles for the intracellular delivery of siRNA. *Int J Nanomedicine.*  
729 2013;8:2041–52.

730 39. Kumirska J, Czerwicka M, Kaczyński Z, Bychowska A, Brzozowski K, Thöming J, et al. Application  
731 of spectroscopic methods for structural analysis of chitin and chitosan. *Mar Drugs.* 2010;8:1567–636.

732 40. Esquivel R, Juárez J, Almada M, Ibarra J, Valdez MA. Synthesis and characterization of new  
733 thiolated chitosan nanoparticles obtained by ionic gelation method. *Int J Polym Sci.* 2015;2015.

734 41. Goulart C, Rodriguez D, Kanno AI, Silva JLSC, Leite LCC. Early pneumococcal clearance in mice  
735 induced by systemic immunization with recombinant BCG PspA-PdT prime and protein boost correlates  
736 with cellular and humoral immune response in bronchoalveolar fluids (BALF). *Vaccine X.* The  
737 Author(s); 2020;4:100049.

738 42. Alonso MJ. Nanomedicines for overcoming biological barriers. *Biomed Pharmacother.* 2004;58:168–  
739 72.

740 43. Singh Y, Meher JG, Raval K, Khan FA, Chaurasia M, Jain NK, et al. Nanoemulsion: Concepts,  
741 development and applications in drug delivery. *J Control Release.* Elsevier B.V; 2017;252:28–49.

742 44. Goycoolea FM, Valle-Gallego A, Stefani R, Menchicchi B, David L, Rochas C, et al. Chitosan-based  
743 nanocapsules: Physical characterization, stability in biological media and capsaicin encapsulation. *Colloid*  
744 *Polym Sci.* 2012;290:1423–34.

745 45. Calvo P, Alonso MJ, Sur C. Development of positively charged colloidal drug carriers : chitosan-  
746 coated polyester nanocapsules and submicron-emulsions. 1996;

747 46. Gradauer K, Vonach C, Leitinger G, Kolb D, Fröhlich E, Roblegg E, et al. Chemical coupling of  
748 thiolated chitosan to preformed liposomes improves mucoadhesive properties. *Int J Nanomedicine*.  
749 2012;7:2523–34.

750 47. Maruyama CR, Guilger M, Pascoli M, Bileshy-José N, Abhilash PC, Fraceto LF, et al. Nanoparticles  
751 Based on Chitosan as Carriers for the Combined Herbicides Imazapic and Imazapyr. *Sci Rep. Nature*  
752 *Publishing Group*; 2016;6.

753 48. Shrestha S, Wang B, Dutta P. Nanoparticle processing: Understanding and controlling aggregation.  
754 *Adv Colloid Interface Sci. Elsevier B.V.*; 2020;279:102162.

755 49. González-Aramundiz JV, Peleteiro M, González-Fernández Á, Alonso MJ, Csaba NS. Protamine  
756 Nanocapsules for the Development of Thermostable Adjuvanted Nanovaccines. *Mol Pharm*.  
757 2018;15:5653–64.

758 50. Tuoriniemi J, Johnsson ACJH, Holmberg JP, Gustafsson S, Gallego-Urrea JA, Olsson E, et al.  
759 Intermethod comparison of the particle size distributions of colloidal silica nanoparticles. *Sci Technol*  
760 *Adv Mater. IOP Publishing*; 2014;15.

761 51. Menchicchi B, Fuenzalida JP, Bobbili KB, Hensel A, Swamy MJ, Goycoolea FM. Structure of  
762 Chitosan determines its interactions with mucin. *Biomacromolecules*. 2014;15:3550–8.

763 52. Collado-González M, Espinosa YG, Goycoolea FM. Interaction between Chitosan and Mucin:  
764 Fundamentals and applications. *Biomimetics*. 2019;4:1–20.

765 53. He F, Becker GW, Litowski JR, Narhi LO, Brems DN, Razinkov VI. High-throughput dynamic light  
766 scattering method for measuring viscosity of concentrated protein solutions. *Anal Biochem. Elsevier Inc.*;  
767 2010;399:141–3.

768 54. Raskin MM, Schlachet I, Sosnik A. Mucoadhesive nanogels by ionotropic crosslinking of chitosan- g  
769 -oligo(NiPAam) polymeric micelles as novel drug nanocarriers. *Nanomedicine*. 2016;11:217–33.

770 55. Szymańska E, Winnicka K. Stability of chitosan - A challenge for pharmaceutical and biomedical  
771 applications. *Mar Drugs*. 2015;13:1819–46.

772 56. Tonglairoum P, Brannigan RP, Opanasopit P, Khutoryanskiy V V. Maleimide-bearing nanogels as  
773 novel mucoadhesive materials for drug delivery. *J Mater Chem B*. 2016;4:6581–7.

774 57. Kaldybekov DB, Tonglairoum P, Opanasopit P, Khutoryanskiy V V. Mucoadhesive maleimide-  
775 functionalised liposomes for drug delivery to urinary bladder. *Eur J Pharm Sci*. Elsevier B.V;  
776 2018;111:83–90.

777 58. Tzankova V, Gorinova C, Kondeva-Burdina M, Simeonova R, Philipov S, Konstantinov S, et al.  
778 In vitro and in vivo toxicity evaluation of cationic PDMAEMA-PCL-PDMAEMA micelles as a carrier of  
779 curcumin. *Food Chem Toxicol*. Elsevier Ltd; 2016;97:1–10.

780 59. Mellman I, Steinman RM. Minireview Dendritic Cells: Specialized and Regulated Antigen Processing  
781 Machines cells are adept at endocytosis and express relatively low levels of surface MHC class I and II  
782 products and costimulatory molecules (e.g., CD86). Abundant MHC class II mol-. *Cell*. 2001;106:255–8.

783 60. Banchereau J, Steinman RM. Dendritic cells and the control of immunity. *Nature*. 1998;392:245–52.

784 61. Al-Ashmawy GMZ. Dendritic Cell Subsets, Maturation and Function. *Dendritic Cells*. InTech; 2018.

785 62. Braun D, Longman RS, Albert ML. A two-step induction of indoleamine 2,3 dioxygenase (IDO)  
786 activity during dendritic-cell maturation. *Blood*. 2005;106:2375–81.

787 63. Fallarino F, Grohmann U, Vacca C, Bianchi R, Orabona C, Spreca A, et al. T cell apoptosis by  
788 tryptophan catabolism. *Cell Death Differ*. 2002;9:1069–77.

789 64. Caulfield MJ. Endotoxin-induced T lymphocyte S N Vogel , M L Hilfiker and M J Caulfield  
790 Information about subscribing to The Journal of Immunology is online at : 2019;

791 65. Craig A, Mai J, Cai S, Jeyaseelan S. Neutrophil recruitment to the lungs during bacterial pneumonia.  
792 *Infect Immun*. 2009;77:568–75.

793 66. Dzopalic T, Rajkovic I, Dragicevic A, Colic M. The response of human dendritic cells to co-ligation  
794 of pattern-recognition receptors. *Immunol Res*. 2012;52:20–33.

795 67. Peleteiro M, Presas E, González-Aramundiz JV, Sánchez-Correa B, Simón-Vázquez R, Csaba N, et  
796 al. Polymeric nanocapsules for vaccine delivery: Influence of the polymeric shell on the interaction with  
797 the immune system. *Front Immunol*. 2018;9.

